ARMY RESEARCH LABORATORY

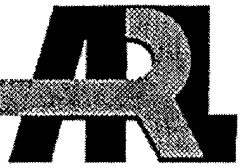

Assessment of Two Electro-Rheological Fluids for Use in Recoil Abatement Applications

by Laszlo J. Kecskes

ARL-TR-2483 May 2001

The findings in this report are not to be construed as an official Department of the Army position unless so designated by other authorized documents.

Citation of manufacturer's or trade names does not constitute an official endorsement or approval of the use thereof.

Destroy this report when it is no longer needed. Do not return it to the originator.

Army Research Laboratory
Aberdeen Proving Ground, MD 21005-5069

ARL-TR-2483 **May 2001**

Assessment of Two Electro-Rheological Fluids for Use in Recoil Abatement Applications

Laszlo J. Kecskes
Weapons and Materials Research Directorate, ARL

Abstract

The electrical and rheological properties of two state-of-the-art electro-rheological (ER) fluids have been evaluated from 0 to 60 °C, using a unique constant-stress viscometer. The measurements were performed at the facilities of ER Fluid Developments, Ltd. (ERFD), a small British company located in Sheffield, United Kingdom, that specializes in developing and marketing ER fluid-based technology. In addition to these measurements, the response time of the fluids was determined using another instrument located at the nearby University of Sheffield.

The constant-stress viscometer, or dynamic rig, developed and owned by ERFD, permits the yield stress, plastic viscosity, and direct current (DC) current density of an ER fluid to be determined as a function of electric field and temperature. The yield stress, plastic viscosity, current density, and response time of each fluid were found to strongly depend on temperature. The first fluid appears to be stronger (i.e., has a higher yield stress), with lower current densities at lower temperatures up to 40 °C. In that temperature range, the second fluid is somewhat weaker, susceptible to electrical breakdown at or above 2.0 $kVmm^{-1}$, and generally draws more current. At higher temperatures, however, the current density of the first fluid dramatically increases to exceed the desired level of 10 μAcm^{-2}. The corresponding current density increase of the second fluid is significantly smaller. In light of the differences between the measured properties, the results and their implications associated with the intended use of the fluids are discussed. A general description of ER fluid behavior, as well as the theories of operation of the instruments, are also described.

Acknowledgments

The author gratefully notes the contributions of Dr. Ross Harder at General Atomics, Corporation for providing the electrorheological (ER) fluid samples to the U.S. Army Research Laboratory (ARL) and for offering the opportunity to perform the measurements; Dr. Jim Stangroom, Dr. Linda Evans, Mr. Peter Kerdmore, and Mr. Ian Harness at ER Fluid Developments, Ltd. in Sheffield, United Kingdom, are thanked for the hospitality, the use of the facility, training, aid with the experiments, data collection and reduction, and interpretation of results. Mr. William Bullough and his staff at the Department of Mechanical and Process Engineering, University of Sheffield, performed the activation/deactivation response time experiments. Also, Dr. Andrus Niiler at ARL and Dr. Sheldon Cytron at the U.S. Army Research and Development Center (ARDEC) are appreciated for their valuable suggestions and discussions.

INTENTIONALLY LEFT BLANK.

Contents

List of Figures

INTENTIONALLY LEFT BLANK.

List of Tables

INTENTIONALLY LEFT BLANK.

1. Introduction

Several Army laboratories, with the lead of the Fire Support Armaments Center, U.S. Army Armaments Research, Development, and Engineering Center (FSAC/ARDEC), Rock Island Arsenal (RIA), U.S. Army Research Laboratory (ARL), and General Atomics Corporation (GA) are currently developing a large-caliber, 155-mm Light Artillery Future Direct Support Weapon System (FDSWS) for Army After Next forces. Since its inception, the FDSWS has been renamed to the Advanced Technology Lightweight Artillery System or ATLAS. Relying on advanced materials and novel recoil abatement technologies, ATLAS is intended to provide lethality and firepower without compromising accuracy, weight, or mobility.

One of the key elements of ATLAS is its use of electro-rheological (ER) fluids to control the recoil action of the gun barrel, wherein the impulse energy imparted by the recoil stroke is managed and dissipated over an expanded time span. A benefit to using ER fluids either directly or indirectly (used as the control fluid for the otherwise nominal howitzer hydraulics) is that when the peak stresses are significantly reduced, the need for the massive undercarriage and supports are lessened.

For ATLAS, an ER fluid with high activity (high shear strength), low no-field viscosity, low current density, and fast response time over a wide temperature range is desired. Additionally, the fluid should be nontoxic, noncorrosive, nonsettling, and compatible with a variety of common engineering materials. Table 1 summarizes these "benchmark," minimum property values.

Table 1. Desired benchmark properties of candidate ER fluids.

Property	Target Value	Conditions
Activity or Yield Strength; τ_y	4 kPa	4 kV/mm; 20 °C
Direct Current (DC) Density; j	< 10 μA/cm^2	0–40 °C
Zero-Field Viscosity; η_0	< 120 mPa•s	20 °C
Response Time; t_r	2 ms	0–40 °C
Nontoxic, noncorrosive, and nonsettling		
Compatible with Aluminum, Titanium, Stainless Steel, Delrin, etc.		

In the past, ER fluids have been applied to automotive engine mounts, clutches, valves, vibration and noise reduction control mechanisms, and liquid crystal displays. However, there are currently still no significant military applications in use [1]. Although several fluids are now commercially available, they tend to be highly design specific. That is, due to its highly specific properties, one fluid used in one application may not be suitable in another. Furthermore, data representing the fluid characteristics is often incomplete, so an accurate property assessment cannot be made. Occasionally, such data may not even be available from the supplier because of a lack of proper instrumentation for its determination. Consequently, ARL has been tasked to develop an in-house evaluation capability to assess ER fluids on a comparative basis, as well as create a comprehensive engineering property database for ER fluids.

Since the FY95–FY96 timeframe, GA worked under contract with FSAC towards designing, constructing, and testing a lightweight, full-scale, ER fluid-based, soft-recoil arrest simulator and its associated control system [2, 3]. With the soft recoil system fitted onto a test bed, live-fire testing was to commence to demonstrate the feasibility of closed-loop, real-time control of a howitzer using ER fluids. Previously, GA and its subcontractor, ER Fluid Developments, Ltd. (ERFD), in Sheffield, United Kingdom, have already built and tested a proof-of-principle subscale device for FSAC that has essentially demonstrated the feasibility of the ER fluid soft-recoil concept [3]. ERFD has been developing ER fluids and associated applications for over 30 years.

In the fall of 1996, a request-for-quote (RFQ) was placed by GA for an ER fluid that could meet the benchmark requirements of the ATLAS program. Two candidate samples were submitted in December 1996. GA was to downselect one of the fluids for ATLAS after a thorough property assessment. GA requested that ARL, acting as an independent, disinterested "third" party, measure the key physical properties of the fluids. However, at that time, ARL still lacked the proper instrumentation and facilities for the evaluation. Therefore, GA suggested and arranged for ARL to perform the necessary measurements by working with ERFD in England.

Test requirements, instructions for handling, and fluid samples were shipped to ARL and, in February 1997, the author traveled to ERFD to perform the measurements. The fluid identities and their respective suppliers were known only to GA. This was crucial for providing a comparative but anonymous basis for experimentation while maintaining confidentiality and impartiality.

Because of time restrictions, the evaluation effort primarily concentrated on the properties of shear stress, viscosity, and current density as a function of electric field intensity, shear rate, and temperature. ERFD's constant stress rheometer, or dynamic drop viscometer, was used to measure the current density, plastic viscosity, and shear strength of the ER fluids as a function of temperature. In a separate series of experiments, the response time of the fluids was measured

under a variety of conditions. These latter tests were performed at University of Sheffield's Department of Mechanical and Process Engineering, Smart Machines, Materials, and Related Technologies (SMMART) Laboratory. Similar to the viscometry experiments, the scope of these tests was to examine the effects of shear rate, electric field intensity, and temperature. This report enumerates the results of both of these series of experiments and describes the devices used for their determination.

2. ER Fluid Characteristics

This section is primarily intended to provide a basis for interpretating test results by the uninitiated. The subject of ER fluids has been extensively covered over the last 30 years, and several excellent review articles have appeared in the literature [4–9].

Currently, only a handful of manufacturers in the United States and abroad have the capability to produce batch-size quantities (i.e., more than a few liters at a time) of ER fluids. In the United States, Bayer Corporation (Pittsburgh, PA) and Bridgestone-Firestone Corporation (Akron, OH) are still active. In Europe, DEA Mineraloel AG (Hamburg, Germany) and ERFD (Sheffield, United Kingdom) continue to produce fluids. Actually, in practice, ERFD has made arrangements with Loctite Corporation (Dublin, Ireland) for the exclusive license to manufacture and sell larger quantities of ERFD's fluid formulations. In Japan, Asahi Chemical Industry Company (Fuji-shi, Shizuoka-ken), Fujikura, Ltd. (Koto-ku, Tokyo), and Nippon Shokubai Corporation (Tsukuba, Ibaraki) lead among other manufacturers. Former fluid producers and their subsidiaries, such as Lord Corporation (Cary, NC), Lubrizol (Wickliffe, OH), RWE (Wesseling, Germany), and BASF (Ludwigshafen, Germany), etc., have either discontinued their research and development efforts, or are continuing them on a greatly scaled-back level.

2.1 General Trends

ER fluids are fine particle suspensions in a base liquid. By applying an electric field, they increase in viscosity to the point of becoming almost solid-like, thereby capable of supporting higher shear stress levels than normal fluids. The composition of the conductive, polar particles can range from flour, starch, crystalline cellulose, carbon, polymers with or without attached metal ions, metals, or ceramics (e.g., alumina, silica, titania, zeolites, etc.). The concentration of particles can vary from 10 to 50 volume-percent, while the optimum particle size seems to be between 40 nm and 50 μm. At one extreme, interference from the Brownian motion of ultrafine particles limits the effectiveness, but at the other extreme, large particles suffer from sedimentation, settling, and a slow

response to the electric field. The carrier fluid is a low viscosity, low dielectric constant, high dielectric breakdown strength, low conductivity, nonpolar fluid. Examples include kerosene, mineral oil, silicone (polydimethyl siloxane), greases, aldehydes, or halogenated hydrocarbons. Weiss et al. [7] and Block and Kelly [10] have provided a whole spectrum of different ER fluid formulations.

The base fluid and particulate mixture also includes additives, namely surface agents, and sometimes an activating agent (water or other polar solvents such as alcohols or glycols). One of the roles of surfactants is to provide stability (to deagglomerate and to prevent sedimentation) to the colloidal suspension and particle fluid interface. Another role is to provide the particle surfaces with mobile charge carriers or an artificially large dielectric constant.

The ER effect, either under static or steady shearing conditions, involves organizing the suspended particles into multistranded chains that possess long-range order. The phenomenon of particle fibrillation, or formation into fibrils, and subsequent theory stemming from it, cannot fully account for the effect alone [11]. Specifically, the timescale needed for fibrillation is significantly greater than the typical millisecond response times of fluids. More recent theories agree that the chaining is the result of interparticle electrostatic attraction that arises from the particles polarizing. Whatever the cause of the polarization, in most fluids there is a relatively large permittivity difference (dielectric constant) between the suspended particles and the base fluid. Theories explaining the origin of this polarization include an induced double-layer charge cloud surrounding each particle [12, 13], electro-osmosis-activated water bridge [14], and intrinsic particle polarization by electronic, atomic, rotational, nomadic, or interfacial charge carriers [10].

The viscosity change is reversible, with an activation-deactivation response time of about a few milliseconds. When active, the macroscopic mechanical and electrical properties such as shear stress, viscosity, and current density predominantly depend on factors such as electric field intensity, shear rate, temperature, and composition (particle concentration and morphology).

In light of the desired benchmark properties, a multitude of component parameters must be considered and solved in the engineering and developing of ER fluids. Some of the issues that have seen some recent improvement include (1) the compatibility of the base fluid and particulates, (2) the density and dielectric strength of the base fluid, and (3) the presence of water and other impurities at the fluid/particle interface.

In the past, the increasing demand for higher activity fluids was usually achieved by higher particle concentrations that led to excessive agglomeration, poor dispersability, and sedimentation. Associated with an increased particle concentration is an unwanted increase of the zero-field viscosity of the fluid. Some of these drawbacks have been alleviated by better density matching

between the components. Particles have become less dense, and denser-base fluids have been introduced. In newer fluids, silicone has been replaced by low molecular weight (less than 500) fluorosilicones (i.e., fluorinated silicones). The advantages of fluorosilicones are not only based on their higher densities, but also on their higher dielectric strengths which permit higher electric fields.

Since introducing anhydrous fluids [15, 10], current trends have taken a sharp turn away from using water to activate fluids. Although traditionally water-activated fluids have very high activities, using water caused problems with corrosion, irreproducibility, limited temperature range, and instability. While the amount of water in "substantially" anhydrous fluids is still being disputed, these fluids have made steady progress in improving their activity levels. At the same time, some of these fluids tend to contain precursors (e.g., silicates or zeolites) that are highly abrasive.

Advancement has also been made in synthesizing, fabricating, and processing fluid components with better control over purity, and with particles, over morphology and size distribution. Introducing new types of composite particles (e.g., metal coated polymers) has also resulted in improved density matching as well as reduced current densities.

2.2 Dynamic Shear Stress and Viscosity of the ER Fluid

The mechanical behavior of the ER fluid may be divided into a preyield and a postyield regime [9]. With increasing field intensity, under preyield conditions, the fluid first behaves as a viscous, then as a linear viscoelastic, and finally as a nonlinear viscoelastic solid. Measurements of the complex shear modulus (i.e., storage and loss components) with electric field, strain amplitude, and frequency indicates that the fluid is a relatively lossy system. However, with increasing electric field and frequency, the storage modulus correspondingly increases. Of course, when compared to more common viscoelastic solids, the absolute magnitudes of the storage moduli are considerably less.

Under the postyield regime, ER fluids are usually modeled as a Bingham material. In steady-state shear for a Bingham plastic, the shear stress is defined as

$$\tau(E, \dot{\gamma}) = \tau_y(E) + \mu_p \dot{\gamma}, \tag{1}$$

where τ_y is an electric-field-dependent yield stress, μ_p is plastic viscosity, and $\dot{\gamma}$ is the shear strain rate. Typical experiments measure the shear stress as a function of shear strain rate. The intercept and slope correspond to τ_y and μ_p. Without an electric field, there is no ER effect and fluid behavior is Newtonian. Some fluids may show a small zero-field yield stress, though. Thus, to a good approximation, τ_y is zero, and μ_p is equal to the Newtonian viscosity, μ. This is also the viscosity at zero-field, μ_0, which is used to characterize the fluid.

Unlike the static yield stress which varies linearly with the applied field intensity, the dynamic yield stress of an ER fluid can be modeled by a power law, but usually a simple parabolic relation is sufficient [5, 16, 17],

$$\tau_y = AE^2. \quad (2)$$

The proportionality constant, A, quoted in [kPa$(kVmm^{-1})^{-2}$], can be used as the fluid performance index. A value of 0.25 for A implies a yield stress of 4 kPa at an electric field of 4kVmm^{-1}. A has been found to vary with fluid and temperature.

While the yield stress defines the upper limit of shear stress that an ER fluid can essentially support, the zero-field viscosity of an ER fluid is important because it identifies the minimum shear stress necessary to initiate flow. The temperature dependence of the zero-field viscosity of ER fluids is similar to that of pure oils (i.e., it monotonically decreases with increasing temperature) [18]. The temperature dependence of the plastic viscosity is similar, and it varies with the square of the electric field. However, the correlations between such relations are not as good as those for the yield stress.

2.3 DC Current Density of the ER Fluid

Knowing the current density of a fluid is critical because it reflects the expected heat load into the fluid and thereby affects its temperature stability. Ultimately, the current density determines the high voltage power demand by the ER-based device. Because of the inherent nature of the various forms of polarization mechanisms, conduction in ER fluids is non-Ohmic.

The measurements of current density are fitted to quadratic empirical relation

$$j = 0.1\,(P \bullet E + Q \bullet E^2), \quad (3)$$

where j is current density, E is the field intensity, and P and Q are constants found by regression analysis. PE appears to be reminiscent of an Ohmic conduction term. Origins of the QE^2 term may be rooted in Coulombic interactions between particles. The role of the 0.1 is rather arbitrary, primarily for convenience. Thus, a Q value of 10 results in 16 μAcm^{-2} at 4 kVmm^{-1}.

Q is also function of the temperature through an Arrhenius-type relation,

$$Q = Q_0 \exp[-\Delta H(RT)^{-1}], \quad (4)$$

where R is the Universal Gas Constant and 8.314 J$(mol\ K)^{-1}$ and ΔH represents an activation energy over a barrier that must be overcome in ER fluid conduction. For fluids that obey this relationship, logQ is a linear function of the inverse absolute temperature. For water activated fluids, logQ is a linear function of the water content of the particulate solid as well.

It is intuitively obvious that in a practical situation, an uncontrolled ER fluid with a large current density may be subject to a thermal runaway effect. That is,

once a fluid can no longer be in thermal equilibrium (i.e., the heat generated during continuous shearing cannot be transported out), the ensuing temperature rise will necessitate increased power levels to maintain the same shear stress levels. In turn, this will generate larger currents.

Varying A with temperature can be brought about indirectly by varying logQ with temperature (i.e., varying Q by changing the temperature, or varying Q by changing the water content). Both have the same effect on A within the limits of experimental error.

2.4 Response Time of the ER Fluid

The activation response time is linked to the formation, breaking, and reforming of particle chains. Conversely, the deactivation response time reflects the rate of relaxation of these chains in the fluid. Since the strength of particle interaction is determined by the extent of polarization, the response time primarily depends on the applied field. It also depends on the concentration and size of the particles, as well as the zero-field viscosity of the base fluid that affect the extent of crowding and ease of particle movement.

3. Description of the Instrumentation

The mechanical property measurements of ER fluids fall along one of two methods: (1) sliding plate mode and (2) flow (valve) mode. In the sliding plate configuration, the test sample is constrained between a stationary and a moving plate [16]. Usually in the test, torque (and based on the type of fluid model, the shear stress) induced by the sample's shear resistance on the stationary plate is measured as a function of the (constant or oscillatory) speed of a moving plate and electric field. This type of geometry includes flat parallel plate arrangements and coaxial cylinder tests either in rotary or axial modes. In the flow mode, the plates remain stationary while the test sample is squeezed through. Both methods lend themselves to measuring the preyield and postyield regions of the ER response.

Response time measurement methods include the rheo-optical approach, oscillatory parallel plate rheometry, optical-lever/torque tube technique, and pressure-driven flow device [19, 7]. In all systems, either in moving plate or flow geometry, the rate of rise of shear stress, viscosity, or pressure of the fluid is matched to that of the input voltage pulse, and the corresponding time delay between signals is measured.

3.1 ERFD Constant-Stress Rheometer

Conventional rheometers use torsion springs to determine the drag torque produced by a fluid. A stiff spring, which would be adequate for measuring the torque exerted by an "active" ER fluid, would be too insensitive to measure the same fluid in its "inactive" zero field state. The relatively low shear rates, which are needed for realistic measurements and achieved in such instruments, also lead to excessive heating and cause the fluid to rapidly overheat.

ERFD has built a Couette geometry device that does not use torsion springs to determine the exerted torque. Owing to its design, the measurement of the yield stress is absolute, depending only on the apparatus dimensions and the applied stress. Similarly, there is no stick-slip (problems at low rotational speeds, i.e., rheopexy), so resonances common with torsion springs are also avoided. Viscosities as low as 30 mPa and yield stresses up to 7 kPa can be measured. Because the data acquisition per data set is completed in less than 1 s, there are little or no heating problems associated with continually shearing the ER fluid.

The operational principle of the dynamic rig is extremely simple. A schematic diagram and photographs of the drop viscometer are shown in Figures 1(a-c). A small (15-30 ml) fluid sample is loaded into a gap between a cup and a rotor. The source of the constant stress is a hanging weight that is attached with a string and wound around the shaft of the rotor. A high voltage applied between the cup and rotor generates an electric field, thereby modifying the fluid viscosity. Thus, when the weight/string is released, the rotor begins to spin. The rotation speed depends on the net acceleration of the falling weight, which in turn is determined by the gravitational constant and the viscous drag in the fluid. As the field intensity increases, the fluid viscosity increases the drag due to the ER effect, , and the rotational speed of the shaft is reduced. An optical wheel and a photodetector monitor the fall rate. The photodetector signal is fed through a data acquisition system into a computer. From the resultant displacement vs. time curves, a fitting routine determines the angular velocity and acceleration, and in turn the shear stress and plastic viscosity of the fluid. The working principles and calibration methodology of the dynamic rig are described in Appendix A.

Since the ER fluid is in series with the high-voltage power supply, the DC current can be simultaneously measured. The current drawn by the fluid is monitored through the internal current meter of the power supply. The current density is then the ratio of the current to the surface area of the rotor. The temperature range of the fluid can be varied from room temperature to 70 °C by using a proportional heater. Temperatures below ambient levels can be reached using a double-walled cup, through which a cooling fluid (e.g., cold water or alcohol-carbon dioxide mixture) can be circulated. At the same time, the shaft and upper bearings are thermally shielded and insulated from the cup and rotor to maintain a constant temperature.

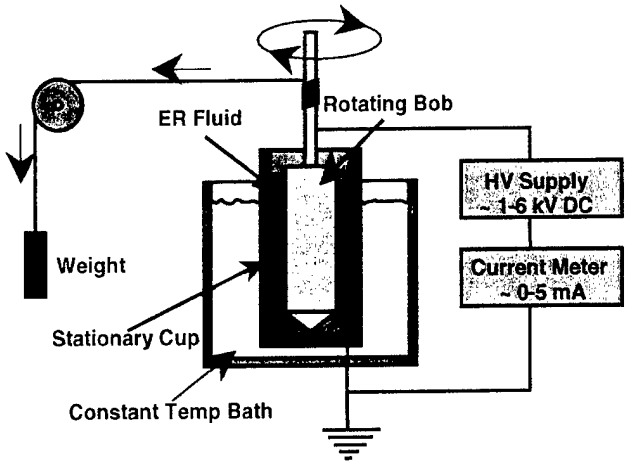

(a)

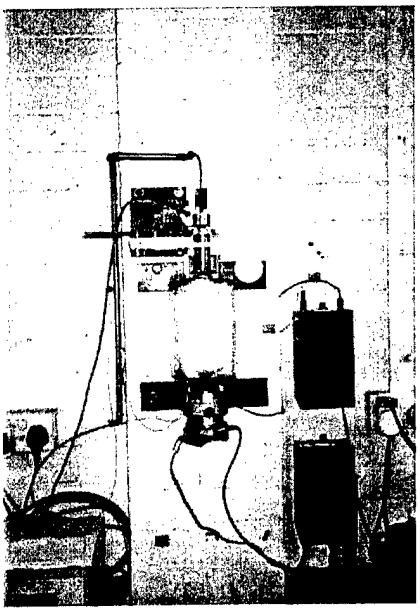

(b)

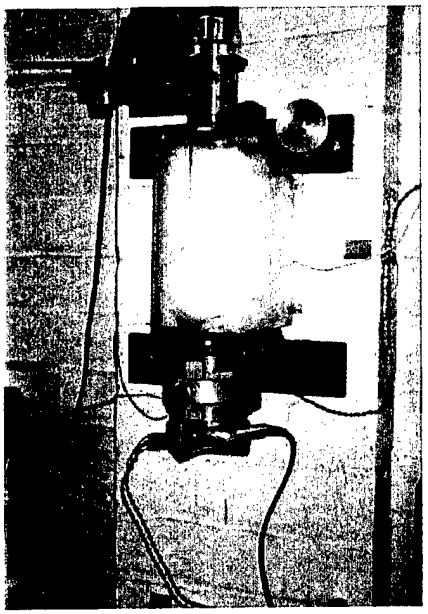

(c)

Figure 1. (a) Schematic diagram of the dynamic drop-viscometer, (b) a photograph of the device, and (c) a close-up.

3.2 Response Time Measurements

The response time tests were performed on a counter-rotating, double-cup ER, clutch-winding rig [20, 21]. The ER clutch is one among four devices at the University available for response time determinations [20, 21]. The winding rig is designed to give a quick general overview of the fluid characteristics. The loading and unloading time response can be observed by comparing the speed of the winding system with the speed of the applied excitation. The rate of acceleration of the belt provides some indication of the yield stress magnitude. The range of shear rates is 0 to about 15,000 s^{-1}. Because of the presence of large

centrifugal forces, the rig can be used to identify problems associated with fluid settling. A range of temperatures can be covered; however, for temperatures above 45 °C, an external blower is necessary. See Figure 2 for a schematic diagram of the winding rig.

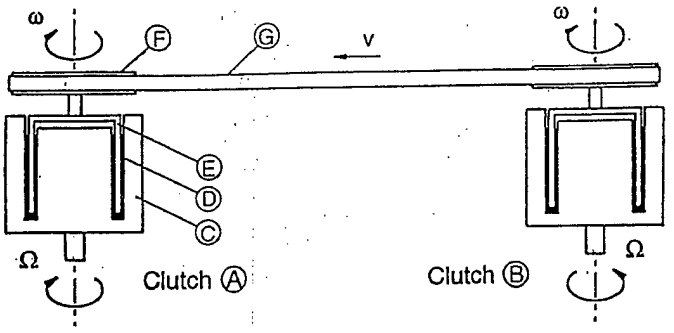

(a)

Cross Section Drawing of E.R. Clutch

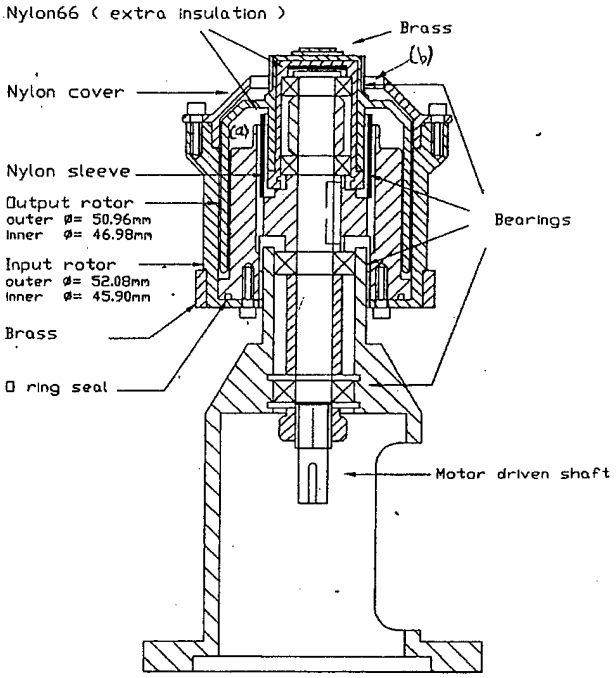

(b)

Figure 2. Schematic diagram of the double ER clutch (A, B) used to measure the response time is shown in (a), with assembly detail in (b). In Figure 2(a), the various components are C - input rotor, D - ER fluid, E - output rotor, F - pulley, and G - drive belt.

The mechanism consists of two vertically mounted ER clutches, A and B, respectively. Each clutch consists of an input (C) and an output (E) rotor. The gap between the two rotors is filled with fluid (D). A pulley (F), attached to the shaft of output rotor of clutch A, is connected by a reciprocating belt (G) to an equivalent pulley on the shaft of the output rotor of clutch B. The motor-driven input rotor runs at virtually a constant speed, which is accomplished because its inertia is much larger than that of the output rotors, pulleys, and belt. Because the inertia of the output rotors, pulleys, and belt are as low as possible, the reciprocating action of the device can respond quickly to changes in the ER torque applied to the clutches. A full cycle is produced by alternatively energizing the A or B clutch. Table 2 summarizes the various segments during the traversing cycle of the winding rig.

Table 2. Conditions during the traversing cycle of the winding rig.

Portion of Belt Motion	Belt Speed	Clutch A			Clutch B		
		Energized	ER Torque	Slipping	Energized	ER Torque	Slipping
0 to 1: constant speed	$-u$	no	no	yes	yes	yes	no
1: excitation A on; B off	$-u$	yes	no	yes	no	no	no
1 to 2: slowing	$-u \le v \le 0$	yes	no	yes	no	no	yes
2: ER torque A on	$-u \le v \le 0$	yes	yes	yes	no	no	yes
2 to 3: slowing	$-u \le v \le 0$	yes	yes	yes	no	no	yes
3: stopped	0	yes	yes	yes	no	no	yes
3 to 4: accelerating	$0 \le v \le u$	yes	yes	yes	no	no	yes
4 to 6: constant speed	u	yes	yes	no	no	no	yes
6: excitation A off; B on	u	no	no	no	yes	no	yes
6 to 7: slowing	$0 \le v \le u$	no	no	yes	yes	no	yes
7: ER torque B on	$0 \le v \le u$	no	no	yes	yes	yes	yes
7 to 8: slowing	$0 \le v \le u$	no	no	yes	yes	yes	yes
8: stopped	0	no	no	yes	yes	yes	yes
8 to 9: accelerating	$-u \le v \le 0$	no	no	yes	yes	yes	yes
9 to 0: constant speed	$-u$	no	no	yes	yes	yes	no

The input rotor cups are motor driven to rotate in opposite directions. If the viscous torques (belt tension and inertial effects) are balanced on both clutches, there is no net torque on the belt, and the output rotors are stationary. Otherwise, the rotors spin either clockwise or counterclockwise. When a step voltage is applied to one of the clutches (i.e., that ER clutch is activated), both

rotors rotate in that direction. If the voltage is turned off and an equal voltage is applied to the other (inactive) clutch, the rotors and belt rotate in the reverse direction. This reversal does not occur instantaneously because of delays in the response times of the power supply, belt hydraulics, and the ER effect. By monitoring the speed of the belt simultaneously with the magnitude of the applied voltage to either clutch as a function of time, the time delay of the belt response can be measured. Because the voltage rise time in the current power supply is rapid (i.e., less than a millisecond), most of the delay could be attributed to the ER response (in the millisecond range) and thus be easily determined. Repeated tachometer measurements and data averaging minimize inertial effects and belt slipping. The ER torque and the electronic-hydraulic time delay are both affected by temperature, shear rate, and field intensity.

4. Experimental Procedure

4.1 ERFD Constant-Stress Rheometer

Operating the viscometer was relatively straightforward. Initially, the heaters, power supply, and computer were turned on. The upper heater, controlling the temperature of the capstan shaft, was set at a constant value of 30 °C, while the lower heater, controlling the temperature of the rotor, holding cup, and fluid, could be varied between 30 and 70 °C. The fluid sample was pippetted into the gap between the rotor and cup. After ensuring that no air bubbles remained in the fluid, the temperature was set. Usually, the temperature of the cup and fluid equilibrated about 30 min after its value was set at the proportional heater. Six temperatures were chosen: 5, 15, 30, 40, 50, and 60 °C. For the temperatures below ambient conditions, a jacketed cup was used that permitted cold tap water to circulate.

Prior to a drop, the string, attached to the pan holding a 10-lb dropweight, was wound up around the capstan. A holding clamp was used to lock the weight into position. The high voltage was turned on, and the data logger was engaged to receive data. By releasing the holding clamp, the weight was then dropped. The total DC current drawn through the fluid was recorded, and the high voltage was turned off. During each drop, 600 time-pulse data points were taken and recorded. A set of six drops was taken for each electric field increment. Between the successive drops, the shaft was rotated 60° counterclockwise, which was necessary for averaging any circumferential nonuniformities around the shaft and bearings of the device.

The power supply voltage was incremented from 0.0 to 2.0 kV in steps of 0.25 kV, which corresponded to a field intensity of 0.5 $kVmm^{-1}$ at the gap. The field was ramped until either an electric discharge occurred in the fluid, or the

dropweight did not drop. If the weight did not drop, the shear strength of the fluid exceeded the gravitational force. In those instances, the ramping sequence was terminated.

After completing each dataset, the computer was instructed to extract the data from the logger. Usually, while applying the high voltage, the computer was disengaged from the logger to protect it from any stray high-voltage arcs. This way, if the fluid arced, only the logger was affected. For each dataset, the computer displayed the individual displacement vs. speed trajectories. Trajectories that fell more than ±5% outside of the average were typically rejected. A straight-line fit extracted the slope and intercept that could then be converted into shear stress and plastic viscosity with the appropriate calibration factors. See Appendix A for further details.

A new fluid sample was used at each temperature increment. Additionally, if the fluid arced, it was removed from the apparatus. This was necessary because a discharge across the cup/rotor gap usually damaged the rotor surface and produced a hard lump in the fluid. With each fluid replacement, the cup and rotor were rinsed clean with acetone, then wiped clean with a damp cloth to remove any residue. After arcing, the rotor was inspected, and the damaged surface was repaired if necessary.

The DC current was recorded just prior to releasing the weight. The readings from the six consecutive drops were averaged, converted into current density, and a straight line was fitted to data to obtain the value of Q at each temperature. The current drawn by the stationary, nonshearing fluid was usually less than that drawn during shearing. This transient current rise was attributed simply to the rise of the fluid temperature from shearing, since a warmer fluid would draw higher current levels. Hence, the recorded current actually represented a lower limit of the electrical load across the fluid.

Current measurements were unaffected by the breakdown of the fluid by arcing. If arcing occurred that prevented the drop tests from continuing, readings could still be taken as a function of the applied field. In these situations, the rotor was spun around several times by hand to break up the particle aggregates, thereby rehomogenizing the suspension. In these cases, typically only a single current reading was taken. These data were also converted into current densities and included in the regression fit.

ERFD's method of obtaining P and Q from the equation for j is to perform a first-order, linear, least-squares regression to the empirical function

$$jE^{-1} = 0.1\,(P + Q \bullet E). \tag{5}$$

The linear term represents the "customary" Ohmic conduction of the fluid. The quadratic term represents the coulombic interactions in the ER fluid. To a large extent, P can be treated as an artifact of the fitting process [22]. It is the quadratic

term, in which the ER effect is related to temperature through Q, that determines the utility and working range of the fluid.

To examine the effect, any artificially introduced bias of the fit near j = 0.0 (a second-order least squares regression, wherein P and Q are treated independently) was applied directly to j. The results of the two methods to obtain P and Q agreed with each other within the limits of statistical error. The Q values from both methods were then fitted to the exponential Arrhenius temperature function.

4.2 Response Time Measurements

The amount of fluid available for testing was limited. Therefore, only a few different conditions could be tried; Table 3 identifies these conditions. In all cases, the signal frequency of the input rotors was a 2-Hz binary square wave of either ±1 or ±3 $kVmm^{-1}$. The electric field intensity was based on an input rotor/output rotor gap of 0.5 mm. In addition to those listed in Table 3, a few preliminary tests were conducted. In these, the electric field was applied, but the rig was not rotating; or alternatively, the rig was rotating without any field present.

Table 3. Test matrix for the response time measurements.

Fluid	T (°C)	E ($kVmm^{-1}$)	$\dot{\gamma}$ ($\times 10^3\ s^{-1}$)
1	30	1	4
1	30	1	10
1	30	3	4
1	30	3	10
1	60	1	4
1	60	1	10
1	60	3	4
1	60	3	10
2	30	1	4
2	30	1	10
2	30	3	4
2	30	3	10
2	60	1	4
2	60	1	10
2	60	3	4
2	60	3	10

A ballast resistor of about 50 kΩ was placed in series with the fluid/electrode in each clutch circuit. The resistor did not significantly alter any of the results. But

it did prevent breakdown or arcing from occurring, thereby giving a degree of security to the test.

An infrared thermometer was located on the outer case of the input rotors. The fluid temperature was assumed to be this value. The ambient temperature ranged from 20 to 23 °C. The belt speed, measured by a tachometer, was directly fed into the digital oscilloscope. Because of the characteristic noise of the winding rig system, typically 64 readings of the tachometer output were signal averaged. The on/off excitation response of the two clutches was determined to be identical. As a result, only one side of the response was measured at the various field strengths, shear rates, and outer case temperatures. Any imbalance in excitation, temperature, or shear rate would have caused the rig to move unsymmetrically. This was quite expected, since the response time depends on all three variables.

The measurement data from the SMMART laboratory was provided in raw format as a series of graphical plots of traces of both input and output signals as a function of time for one of the ER clutches. For each set of conditions enumerated in Table 3, several graphs were provided with varying degrees of detail of the voltage signals. The delay times were determined graphically by measuring the elapsed time along the horizontal time scale from the onset of the sharp drop at the trailing edge of the input voltage to the point where the belt began to decelerate (and accelerate in the reverse direction). The deceleration rate of the belt, which is qualitatively related to the fluid yield stress, was also determined.

5. Results and Discussion

The limited number of currently available ER fluid formulations with their unique physical characteristics, such as color and odor of fluid and/or color of suspended particles, make it relatively easy to correctly identify the supplier or manufacturer of a particular fluid. While these features constitute a significant part of a characterization effort, it would offer a "dead give-away" in guessing a fluid's composition. Therefore, these aspects have been purposely omitted to render the comparative measurements more unbiased.

During viscometry, Fluid 1 was fairly well behaved. That is, this fluid only began to break down (arc [discharge] across the gap between the rotor and cup) at the highest temperatures. However, Fluid 2 prematurely arced at all temperatures, and more importantly, at relatively low electric fields. (An interfacial breakdown between the carrier oil and particulates in the fluid was suspected. The actual reason, traced to contaminants in the oil, was only revealed by GA and the fluid manufacturer at a much later time.)

5.1 ERFD Results

The constant-stress rheometer was used to measure the DC current density drawn by each fluid, yield stress, and plastic viscosity. The results of the current measurements will be discussed first, followed by the stress and viscosity measurements.

DC Current Density. Results of the current density measurements for Fluid 1 are summarized in Table 4 and plotted in Figures 3–5 as a function of electric field and temperature. Data for Fluid 2 are tabulated in a similar fashion as those for Fluid 1 in Table 5 and in Figures 6–8. Listed in the tables are the Q and P values (Coulombic and Ohmic conductions, respectively) from the ERFD and ARL least squares fits to each set of current density data as a function of field intensity and temperature. In each set of three figures, the first two plots depict the behavior of the current density (j) and current density per unit field (JE^{-1}) with field (E), while the third plot depicts the behavior with temperature (T).

Table 4. Fluid 1 current density coefficients.

Temperature			P		Q	
			ERFD	ARL	ERFD	ARL
°C	K	K^{-1}	$(\mu Acm^{-2})(kVmm^{-1})^{-1}$		$(\mu Acm^{-2})(kVmm^{-1})^{-2}$	
5	278.16	0.003,595	-0.072	-1.54	1.13	1.41
15	288.16	0.003,470	-1.42	-3.03	2.44	3.00
30	303.16	0.003,299	-4.03	-5.96	9.93	10.65
40	313.16	0.003,193	-5.36	-6.28	15.59	15.96
50	323.15	0.003,094	-17.59	-43.63	53.48	63.59
60	333.16	0.003,002	-20.04	-61.70	106.94	134.29

Figures 3 and 4 demonstrate the quadratic increase of the current with electric field (i.e., applied voltage) for Fluid 1. Similar graphs in Figures 6 and 7 show the current for Fluid 2. Note that true linear behavior only begins at or above 1.0 $kVmm^{-1}$. These results show two significant differences between the fluids. First, below 40 °C, the current density of Fluid 1 is considerably lower than that of Fluid 2. Second, despite the very low currents at lower temperatures, the rate of rise of the current with temperature for Fluid 1 is significantly greater than that of Fluid 2 (see Figures 5 and 8 for a comparison). Nevertheless, it is quite obvious that Fluid 1 would generate less internal heat than Fluid 2 at or below room temperature.

Fluid 1 Current Density

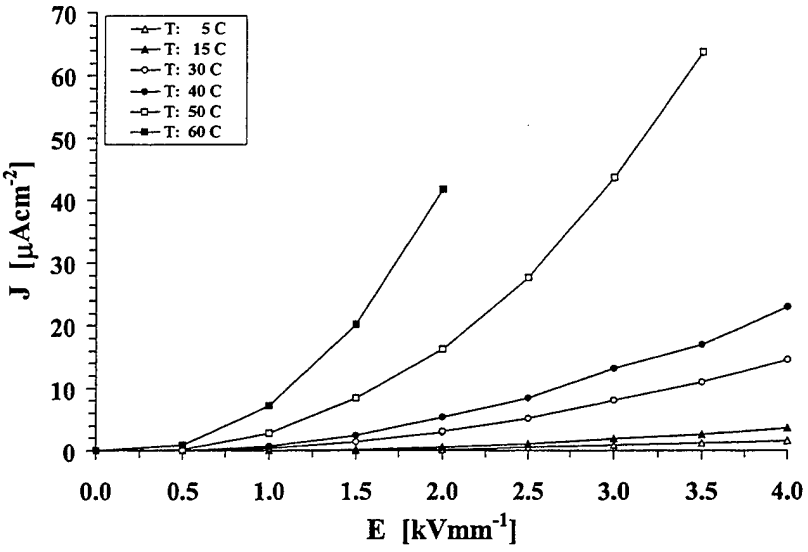

Figure 3. j vs. E; fluid 1.

Fluid 1 Current Density

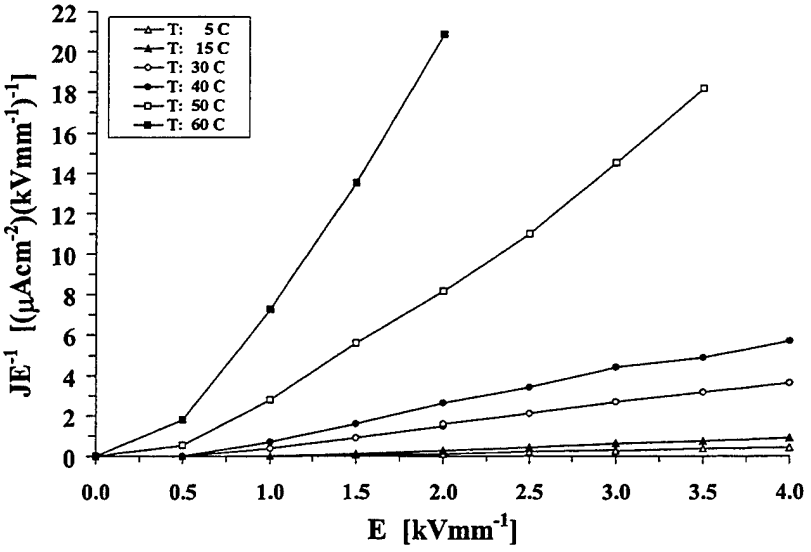

Figure 4. jE^{-1} vs. E; fluid 1.

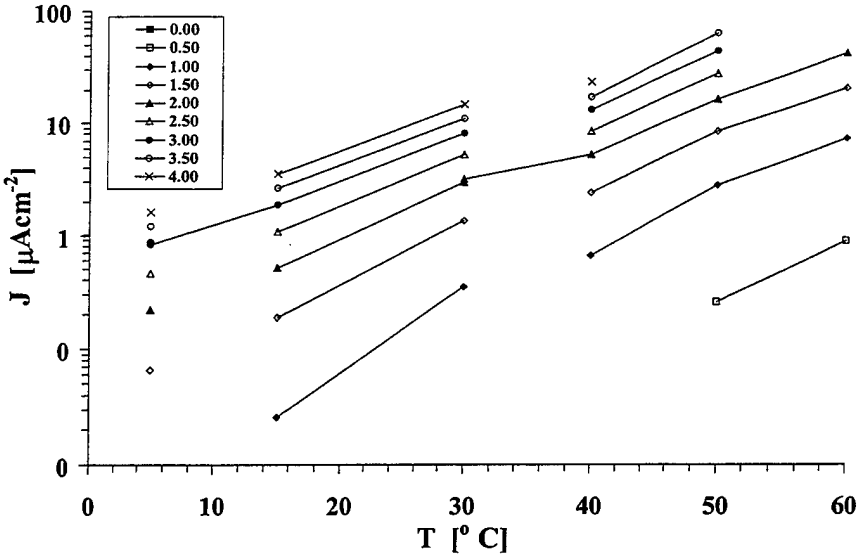

Figure 5. j vs. T; Fluid 1.

Table 5. Fluid 2 current density coefficients.

Temperature			P		Q	
			ERFD	ARL	ERFD	ARL
°C	K	K^{-1}	$(\mu Acm^{-2})(kVmm^{-1})^{-1}$		$(\mu Acm^{-2})(kVmm^{-1})^{-2}$	
5	278.16	0.003,595	1.62	4.24	8.30	7.12
15	288.16	0.003,470	1.72	4.47	11.27	9.80
30	303.16	0.003,299	2.62	7.84	19.49	16.05
40	313.16	0.003,193	7.77	19.35	19.31	14.52
40[a]	313.16	0.003,193	8.95	17.91	18.81	15.69
50	323.16	0.003,094	14.55	27.06	21.91	17.45
60	333.16	0.003,002	18.85	38.31	28.39	21.65

[a] Degassed at room temperature.

Fluid 2 Current Density

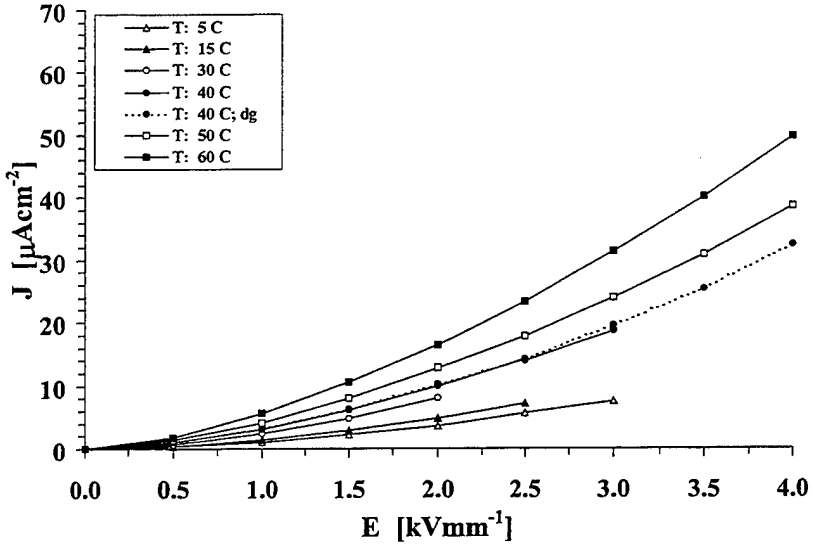

Figure 6. j vs. E; fluid 2.

Fluid 2 Current Density

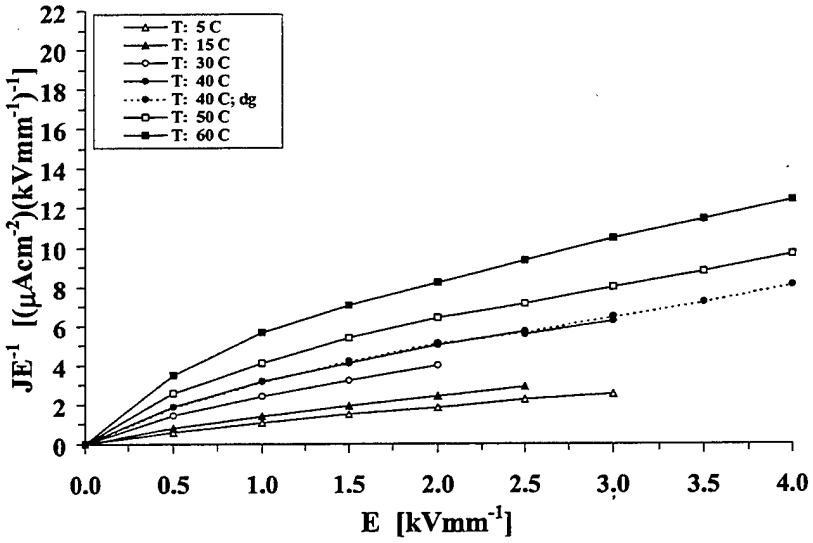

Figure 7. jE^{-1} vs. E; fluid 2.

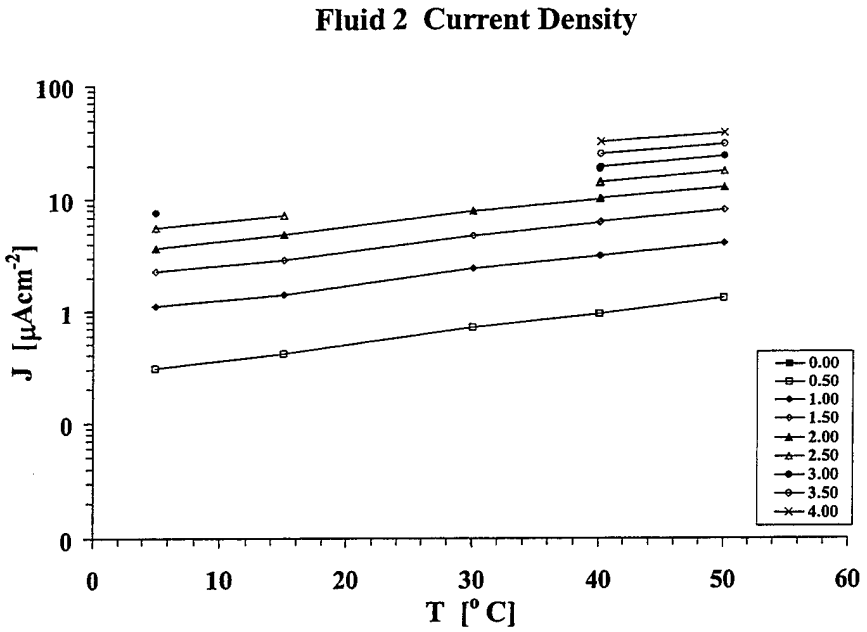

Figure 8. j vs. T; fluid 2.

However, under nonequilibrium conditions such as a thermal runaway scenario, Fluid 2 would heat up more slowly than Fluid 1. This is clearly supported by data in Figure 9, where the logQ is plotted against the reciprocal of the absolute temperature. The straight line generated by a least squares fit is included in the graph. As seen in the graph, both fluids fit well to an Arhenius-type activation process. The current doubling rates and activation energies obtained from the P and Q coefficients are listed in Table 6. Note that the activation energies of the fluids lie between the dissociation energy of a hydrogen bond (about 30 kJ/mol^{-1}) and that of a "true" chemical bond (approximately 400 kJ/mol^{-1}).

The current doubling rate of 8.5 for Fluid 1 is slightly higher than the rate of typical fluids. Since the doubling interval is unique to every fluid and remains fairly constant with temperature, it appears that Fluid 1 was intended to operate below 50 °C. However, probably the most remarkable aspect of Fluid 2 emerges from Table 6. Its current doubling rate is a little more than 30, or roughly 3.5 times the rate of Fluid 1. Thus, at higher temperatures, resistive heating would be significantly lower with its use. This would greatly benefit the design of ATLAS, as lower parasitic heating would reduce the cooling requirements of the ER valve.

Fluid Breakdown Voltage. Table 7 lists the maximum fields supported by each fluid under ambient conditions (standard atmospheric pressure and humidity

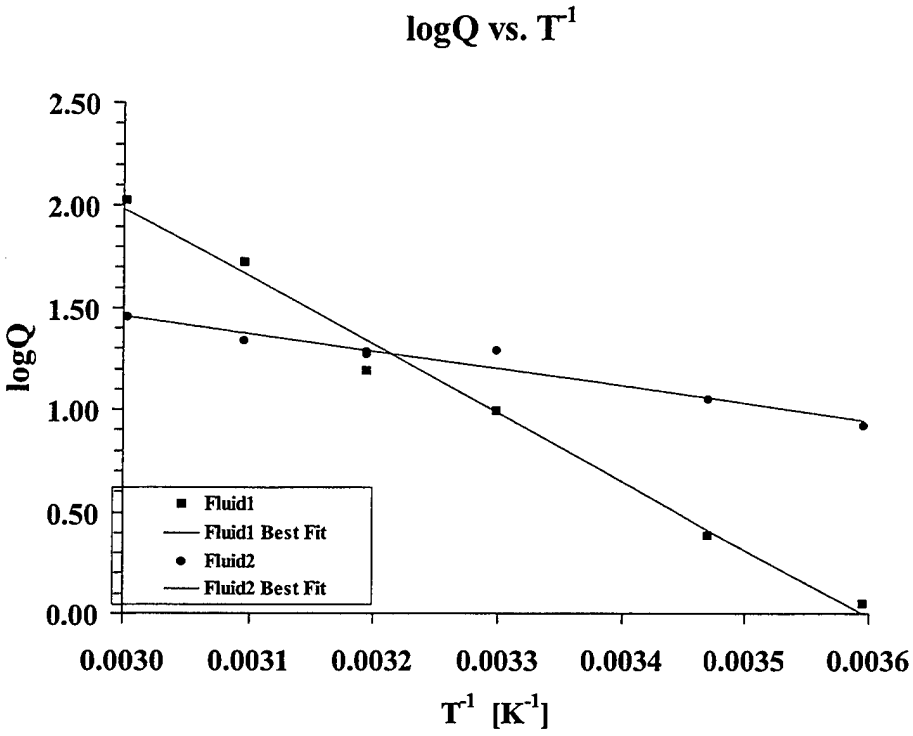

Figure 9. LogQ vs. T^{-1} for both fluids.

Table 6. Fluid current doubling rate and activation energy.

Fluid	Current Doubling Rate at 4 kVmm^{-1} and 300 K	ΔH kJ
1	8.5	63 ±5
2	30.8	15 ±2

level) during testing. It may be assumed with certainty that in cases where the weight did not drop, the maximum field supported by the fluid would be at least 0.5 kV or higher. With the exception of the arcing at the highest temperature (60 °C), Fluid 1 behaved well over the entire temperature range. In contrast, Fluid 2 could not withstand the applied field and broke down at much lower voltages. This shortcoming seriously compromised the course and relevance of the testing.

The most likely cause of arcing is a weak, low-resistance path at the particle/base-fluid interface that allows an electric discharge to form between electrodes. During testing, several explanations arose for the failure of Fluid 2.

Table 7. Fluid breakdown voltage.

T (°C)	$V_{breakdown}$ ($kVmm^{-1}$)	
	Fluid 1	Fluid 2
5	Weight held at 3.0	Arced at 3.0
15	Weight held at 3.0	Arced at 2.5
30	Weight held at 4.0	Arced at 2.0
40	Weight held at 4.0	Arced at 2.5 and 3.0
40[a]	Not Applicable	Arced at 2.5
50	Weight held at 3.5	Arced at 1.5
60	Arced at 2.0	Arced at 1.0

[a] Degassed at room temperature.

Approximately equal amounts of both fluids were air shipped by GA to ARL. On arrival, the bottle containing Fluid 2 was collapsed (i.e., was under partial vacuum). Presumably, a significant fraction of the air was inadvertently adsorbed onto the particle surfaces during shipment from San Diego, CA, to Aberdeen Proving Ground, MD. The fluid was degassed for a few hours with a single-stage rotary pump to extract most of the dissolved air. Since this pump would likely not remove dissociated gases, this method was treated with skepticism. As such, during the evacuation with the roughing pump, only a few air bubbles emerged from the fluid. Supported by the lack of improvement in the current data, the effect of degassing resulted in a very slight change of the rheological properties.

An equally harmful pathogen with deleterious effects for the fluid would have been moisture from air. For this, a vacuum bakeout would have sufficed; however, ERFD lacked the facility to perform this operation. Alternatively, it was put forth that perhaps, triggered by various changes in ambient conditions (temperature, pressure, and gaseous contaminants), a tertiary component in the fluid (such as an additive) or surfactant reacted with the base oil, forming a more conductive product layer on the particles. Lastly, it was hypothesized that fundamental problems already existed with the fluid, but because of inadequate or incomplete testing prior to shipment, the breakdown went unnoticed.

Yield Stress and Viscosity. The yield stress data as a function of electric field for Fluid 1 and Fluid 2 are plotted in Figures 10 and 11; the data are plotted against the square of the electric field. As is apparent in the figures, the yield stress of Fluid 1 adheres to the quadratic dependence fairly well, regardless of the temperature. In contrast, adherence to the expected behavior of Fluid 2 is

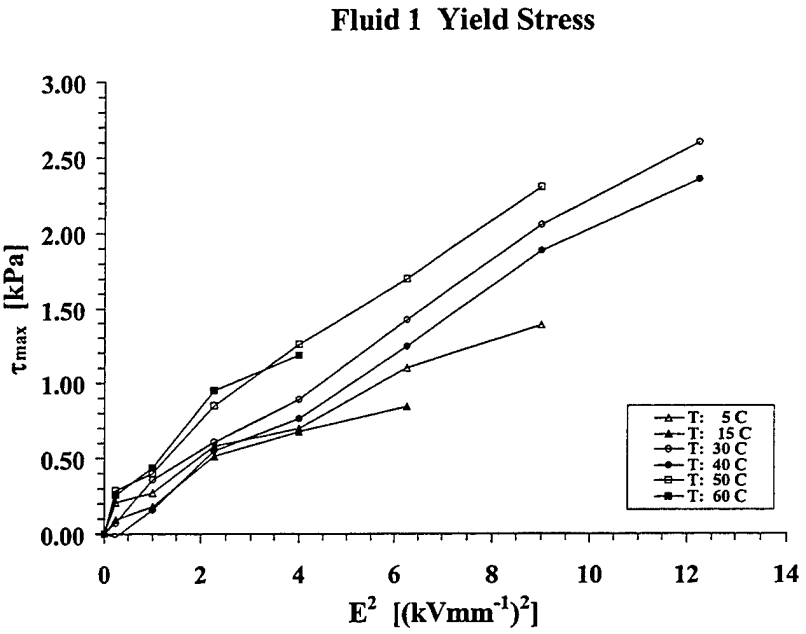

Figure 10. τ_y vs. E^2; fluid 1.

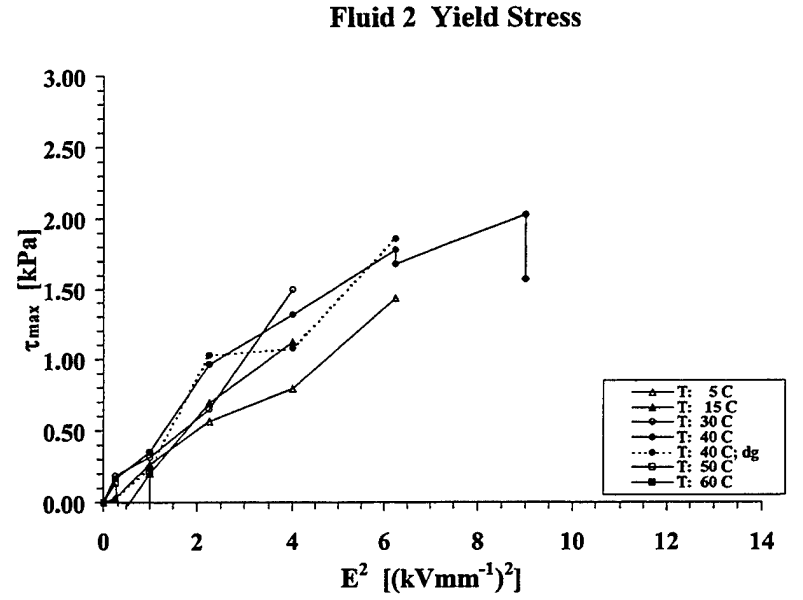

Figure 11. τ_y vs. E^2; fluid 2.

considerably poorer, most likely attributed to its premature breakdown. The deviation from the expected straight-line fit in the latter data is greater, especially at higher temperatures. The arcing and subsequent nonuniform shearing of the arced fluid causes bad drop trajectories and poor fits, which could easily correspond to unrealistic negative yield stress values.

The results in Figure 11 also reveal that the rheological properties of the outgassed fluid did not significantly change from those of the as-received fluid. Similarly, based on the breakdown voltage shown in Table 7, the outgassing treatment did not prevent or delay arcing from recurring either.

Whenever arcing occurred, the damaged fluid was replaced with a new batch of fresh fluid. Consequently, there is considerably more data for Fluid 2 at lower electric fields. Despite the arcing problems, the multiple data values for Fluid 2 reflect fairly good measurement reproducibility.

With increasing temperature (up to 60 °C), the yield stress of Fluid 1 increased slightly. This trend is clearly seen in Figure 12. As revealed by the slope of the lines, at lower field intensities the increase is more gradual. At higher fields, the increase is more pronounced. A similar trend is shown in Figure 13 for Fluid 2. But, for Fluid 2, only data from 0 to 30 °C should be considered in the comparison. Because arcing occurs above this temperature, the data is incomplete and unreliable; therefore, only limited conclusions on the yield stress should be drawn. However, over this restricted range, the rate of increase of the yield stress for Fluid 2 appears to be greater than that of Fluid 1.

The proportionality constant, or the strength factor, A, relating the electric field to the yield stress, was obtained from linear least squares fits to the data plotted in Figures 10 and 11. Generally, as shown in Tables 8 and 9 and Figure 14, the value of A increases with temperature for both fluids. In Table 9, the negative A values are only included for the sake of completeness (i.e., those values that arose from fitting to negative stress values), but they were excluded from the figure. From 0 to 60 °C, A for Fluid 1 increases roughly twofold from 0.15 to about 0.29. It is expected that A will not increase indefinitely, but will reach some asymptotic value. A similar trend was observed for Fluid 2, but its strength factor was considerably higher, reaching values above 0.35. However, for this fluid the electric field could not be increased above 2.5 $kVmm^{-1}$ (see Table 7). As a result, the Fluid 2 fits used to obtain A are based on fewer points; typically, standard errors were about 10–15%, or 3–5 times larger than those for Fluid 1.

The yield stress at an electric field of 4$kVmm^{-1}$ is a critical benchmark for evaluating any ER fluid candidate for recoil applications. However, no actual yield stress data at 4$kVmm^{-1}$ was taken for either fluid. During the attempted drops, Fluid 1 was well behaved and did not arc. In this case, no drop data could be taken because the dropweight did not fall; that is, the ER force was greater than the force of gravity. It is quite reasonable to assume that working with

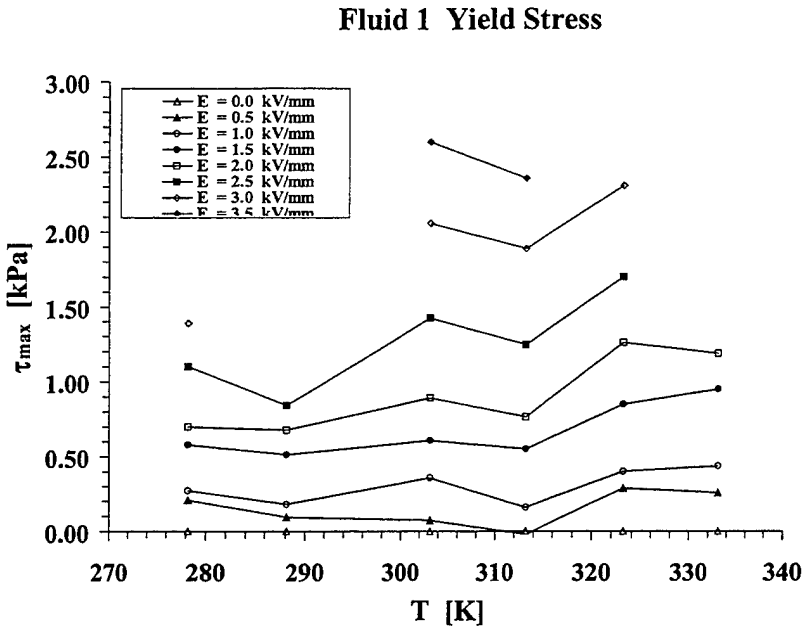

Figure 12. τ_y vs. T; fluid 1.

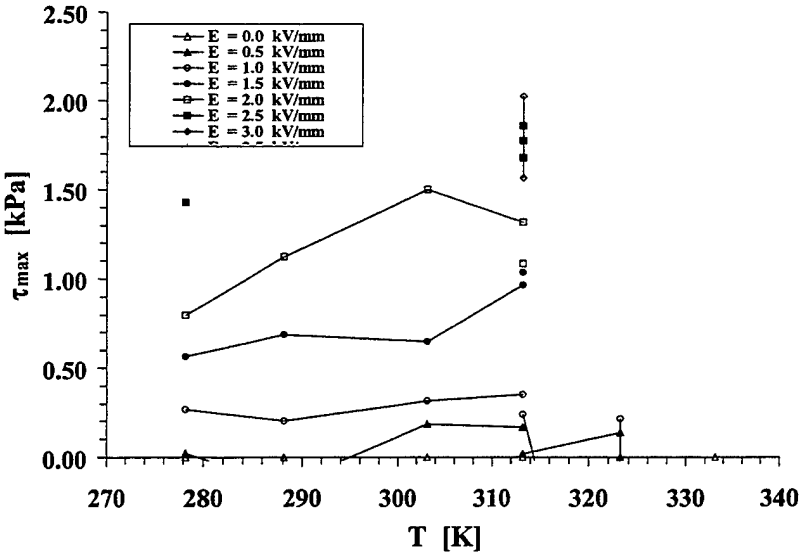

Figure 13. τ_y vs. T; fluid 2.

Table 8. Fluid 1 strength factor, calculated yield stress and no-field viscosity.

T (°C)	E_{max} $kVmm^{-1}$	A $kPa(kVmm^{-1})^{-2}$	τ_y(2 $kVmm^{-1}$) kPa	τ_y(3 $kVmm^{-1}$) kPa	τ_y(4 $kVmm^{-1}$) kPa	η_0 mPa•s
5	3.0	0.15 ± 0.01	0.59	1.3	2.4	350
15	3.0	0.14 ± 0.02	0.55	1.2	2.2	270
30	4.0	0.21 ± 0.01	0.85	1.9	3.4	130
40	4.0	0.20 ± 0.01	0.80	1.8	3.2	-6
50	3.5	0.24 ± 0.01	0.98	2.2	3.9	78
60	2.0	0.29 ± 0.04	1.16	2.6	4.6	9

Note: shaded areas correspond to extrapolated values beyond measurement range.

Table 9. Fluid 2 strength factor, calculated yield stress and no-field viscosity.

T (°C)	E_{max} $kVmm^{-1}$	A $kPa(kVmm^{-1})^{-2}$	τ_y(2 $kVmm^{-1}$) kPa	τ_y(3 $kVmm^{-1}$) kPa	τ_y(4 $kVmm^{-1}$) kPa	η_0 mPa•s
5	3.0	0.22 ± 0.01	0.89	2.0	3.6	60
15	2.5	0.31 ± 0.03	1.26	2.8	5.0	78
30	.0	0.35 ± 0.03	1.41	3.2	5.7	85
40	.5	0.20 ± 0.03	0.80	1.8	3.2	38
40[a]	2.5	0.30 ± 0.04	1.20	2.7	4.8	31
50	.5	-0.96 ± 1.20	—	—	—	22
60	1.0	-0.51	—	—	—	-35

Note: shaded areas correspond to extrapolated values beyond the actual measurement range.
[a] Degassed at room temperature.

larger dropweights would have overcome this minor problem. Unfortunately, due to time considerations, the additional tests with larger dropweights were not performed. Instead, the yield strengths were calculated using equation 2. The calculated yield strength of 3.4 kPa at 4 $kVmm^{-1}$ and 30 °C falls somewhat short of the 4-kPa level.

No such conclusions could be drawn for Fluid 2. The unavailability of high field data, coupled with premature breakdown, seriously compromised the extent of

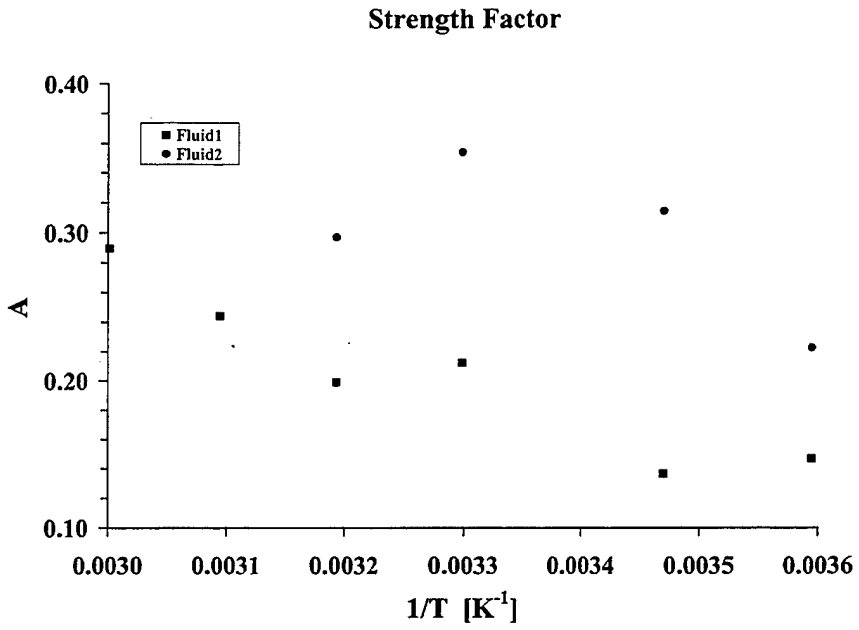

Figure 14. A vs. T^{-1} for both fluids.

the comparative testing. Consequently, the validity of the calculated yield stress for Fluid 2 above 2 $kVmm^{-1}$ is highly controversial. Nevertheless, based on the available low field data, the yield stresses at 3 and 4 $kVmm^{-1}$ were calculated to extrapolate fluid behavior. With that in mind, the projected yield strength of Fluid 2 at 4 $kVmm^{-1}$ and 30 °C was estimated at about 4.0 ± 1.0 kPa, which would be within the desired target range (see Table 9).

For a Bingham fluid, the plastic viscosity, η_P, represents the slope of the family of shear strain rate curves (straight lines) vs. the shear stress, and it decreases with electric field and temperature. Figures 15 and 16 illustrate this behavior quite well for both fluids. For Fluid 1, the range of measured viscosities is very wide. For Fluid 2, the viscosity range is considerably narrower. In both cases, the dependence η_P on the square of the electric field is generally linear. As depicted in Figure 15, the proportionality constant, or the rate of change of η_P, decreases as the temperature increases. This effect is not as clearly observable for Fluid 2 (see Figure 16). The anomalous plastic viscosity datum point at 50 °C was most likely caused by arcing during the measurement which resulted in a bad fit to the trajectory. It was included in the graph for the sake of completeness.

In practical terms, the zero-field viscosity, η_0 (i.e., η_P without an applied electric field), reflects the ease at which the fluid can be pumped through the hydraulic lines of the recoil device. At a more fundamental level, the magnitude of η_0 depends in part on the morphology and the agglomeration tendency of the

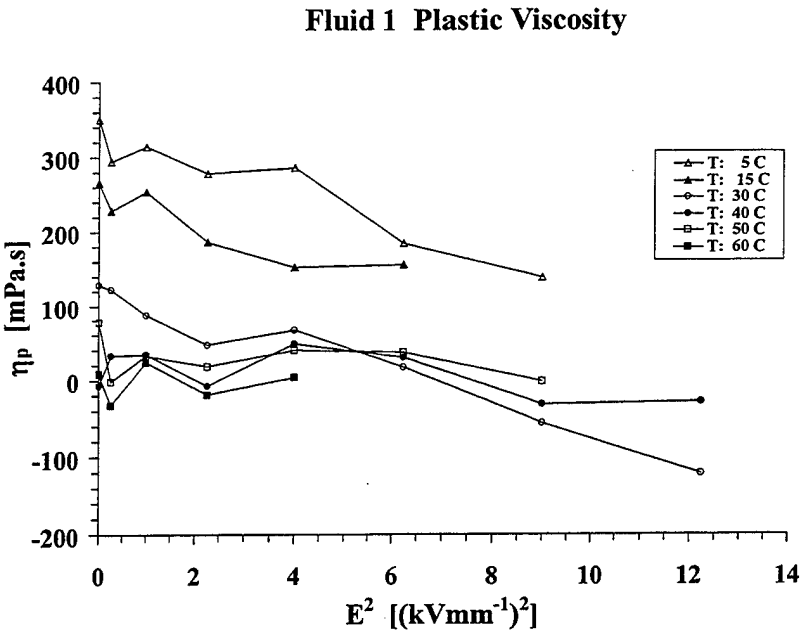

Figure 15. η_p vs. E^2; fluid 1.

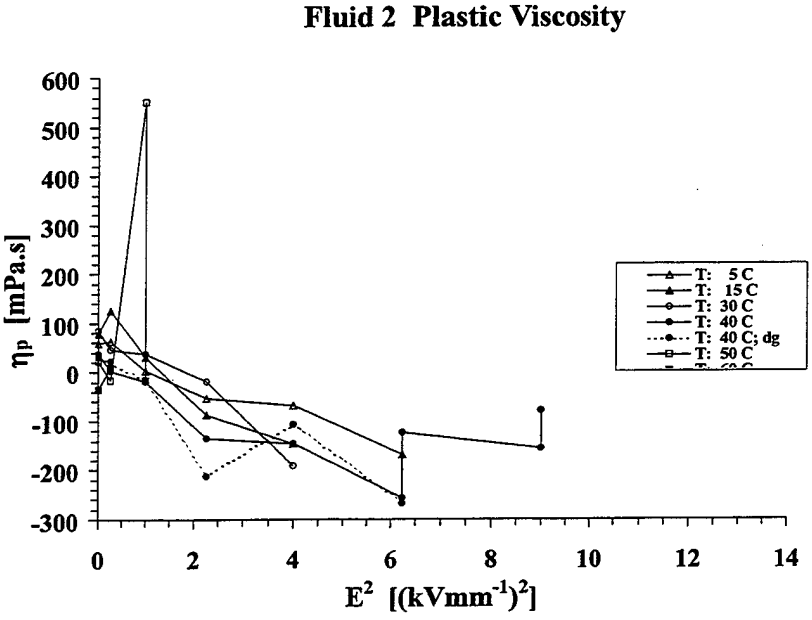

Figure 16. η_p vs. E^2; fluid 2.

particles. However, the base viscosity of the carrier oil, primarily determined by its molecular weight and structure, has a more significant impact on η_0. As expected, Tables 8 and 9 indicate that the two fluids are very different. The experimental errors on the viscosity measurements are about ±10 mPa•s. Determining η_0 is not subject to the issues associated with premature breakdown caused by arcing. The zero or negative values of η_0 are artifacts of the fitting process and would most likely be below the measurement limit of the instrument. As shown in Figure 17, at 0 °C, the viscosity of Fluid 1 is about 350 mPa•s, while at 60 °C it is near 9 mPa•s. In contrast, the viscosity of Fluid 2 is about 60 mPa•s at 0 °C and less than 20 mPa•s at 60 °C. At the lower end of the temperature scale, Fluid 1 is much thicker than Fluid 2. Based on its low temperature viscosity, it is suspected that Fluid 1 would be rather difficult to circulate below 0 °C; however, at higher temperatures, circulation would not be a problem. In contrast, the η_0 for Fluid 2 is not only lower, but also it does not vary as much as that of Fluid 1. In turn, the lower temperature dependence of the fluid viscosity allows the use of a less robust pumping system.

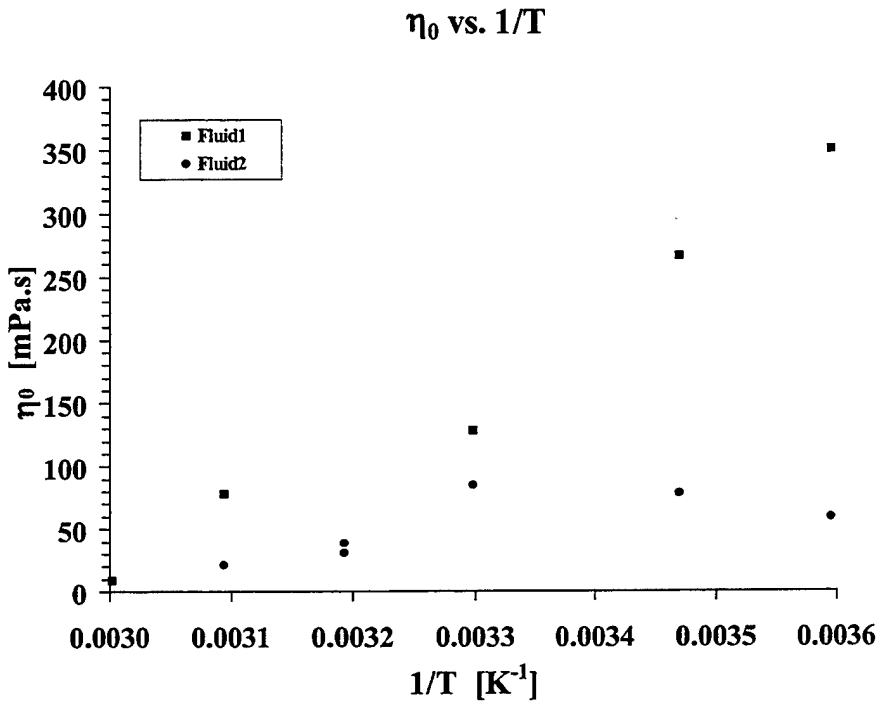

Figure 17. η_0 vs. T^{-1} for both fluids.

Based on the current draw, zero-field viscosity, and extrapolated shear properties, it may be concluded that once corrected, Fluid 2 will be closer to meeting the benchmark conditions than Fluid 1. But it appears that Fluid 1 was

designed to operate within a narrow temperature regime, between 30 and 50 °C. Below this range, the zero-field viscosity is too high, whereas above this range, the current draw is too high. Provided adequate cooling is available, this range could be extended to higher temperatures. However, using Fluid 1 at lower temperatures will be greatly limited by the rapid increase in its zero-field viscosity.

5.2 University of Sheffield Results

Concurrent with the testing at ERFD, samples of both fluids were taken to the SMMART laboratory at the University of Sheffield. Out of courtesy, the laboratory was informed of the premature arcing encountered while testing Fluid 2. Specifically, as a further precaution, the electric field was to be ramped up slowly to the preselected value (e.g., 3 $kVmm^{-1}$) to protect the apparatus. Upon receiving this recommendation, researchers at the SMMART laboratory further consulted with Professor Harry Block of Cranfield University, a known authority on ER fluids. At Block's suggestion, a vacuum bakeout at 80 °C was performed on Fluid 2, which prevented arcing during subsequent winding rig tests.

This rather simple solution implied that the cause of the breakdown was most likely a low boiling point impurity or contaminant in the fluid (i.e., a low molecular weight hydrocarbon or water). This was also consistent with the fact that the impurity could not be removed with a roughing pump at room temperature, but was effectively driven off at intermediate temperatures under better vacuum.

The precautionary step provided a viable remedy for the eliminating/reducing the arcing. However, there was insufficient fluid or time remaining to repeat the entire range of viscometry experiments. More importantly, this action essentially nullified the initial purpose of the measurements—comparative testing of the ER fluids in their as-received states. Preliminary experiments demonstrated that there was little or no interference in the measurements. These tests also indicated that the measurements were repeatable.

Results of the response time measurements are listed in Table 10. A typical example of the oscilloscope traces is also shown in Figures 18(a) and 18(b). In the figure, the upper trace is the DC voltage applied to one of the ER clutches. The lower trace is the tachometer output corresponding to the movement of the belt. Recall that when the applied field on one of the clutches goes to zero, the applied field on the other clutch increases. As shown in the lower trace, the belt is either moving clockwise (CW) (defined as positive) or counterclockwise (CCW). The portion of the lower trace, where the tachometer output linearly increases or decreases, reflects the deceleration and acceleration of the belt associated with reversing the direction of motion. The alternating belt rotation follows switching the DC step voltage (or electric field) input with a slight time delay. On the

Table 10. Response time measurement results.

Fluid	T (°C)	E ($kVmm^{-1}$)	$\dot{\gamma}$ ($\times 10^3\ s^{-1}$)	t_r (ms)	Deceleration Rate (Vs^{-1})
1	32.0	1	4	2.4	34
1	32.5	1	10	3.4	23
1	30.0	3	4	2.6	140
1	34.0	3	10	2.8	240
1	60.0	1	4	2.5	22
1	59.5	1	10	2.5	34
1	62.0	3	4	2.7	45
1	60.0	3	10	2.0	270
2	30.0	1	4	2.0	35
2	32.0	1	10	1.2	5
2	31.0	3	4	2.0	180
2	33.5	3	10	2.1	140
2	60.0	1	4	2.0	39
2	59.0	1	10	2.4	39
2	62.0	3	4	1.6	200
2	60.0	3	10	1.2	190

expanded scale in Figure 18(b), this time delay is clearly apparent. The DC step voltage input usually drops from its constant level to 0 kV within 0.6–1.0 ms. The delay time, t_r, or ER response time, defined as the elapsed time from the onset of the drop of the DC field to the intersection between the linear rise and the horizontal portion of the belt speed trace, was not corrected for the DC voltage decay.

The response time of Fluid 1 varies from 2.0 to 3.4 ms. In contrast, the response time of Fluid 2 is somewhat less, varying from 1.2 to 2.4 ms. The response time also slightly decreases for both fluids with temperature. However, with respect to the applied electric field or shear rate, there is no clear trend. Assuming that all other factors were the same, the deceleration rates listed in the table reflect that there is about a four to six fold increase in the yield stress of the fluids from 1 to 3 $kVmm^{-1}$. This generally agrees with the constant stress viscometer results, which indicated that the yield stress increase from 1 to 3 $kVmm^{-1}$ was roughly a factor of ten. Because the winding rig only gave a quick, general overview of the fluid characteristics, the data was not analyzed or calibrated further.

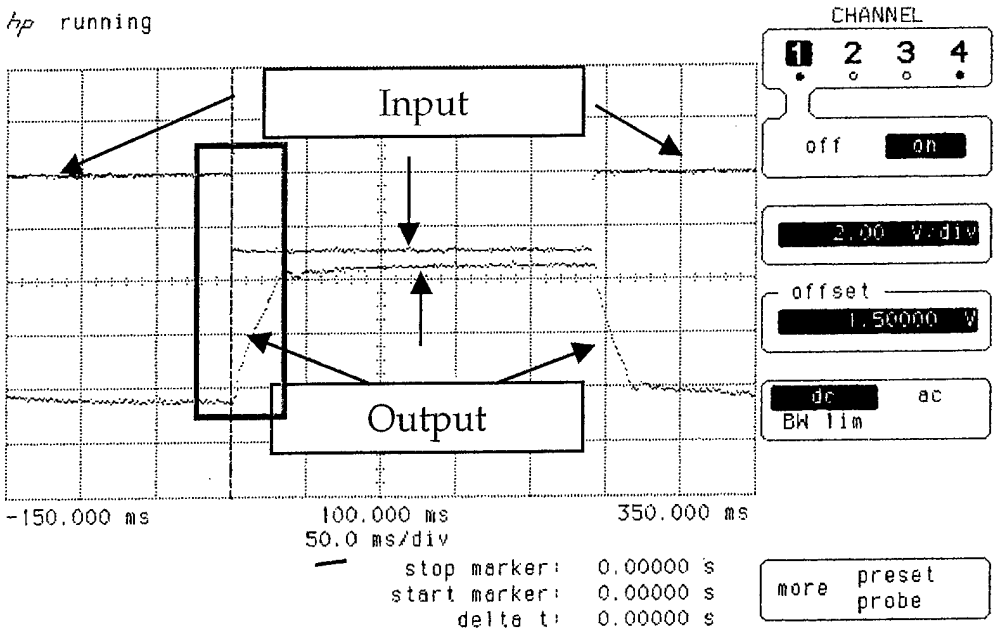

(a)

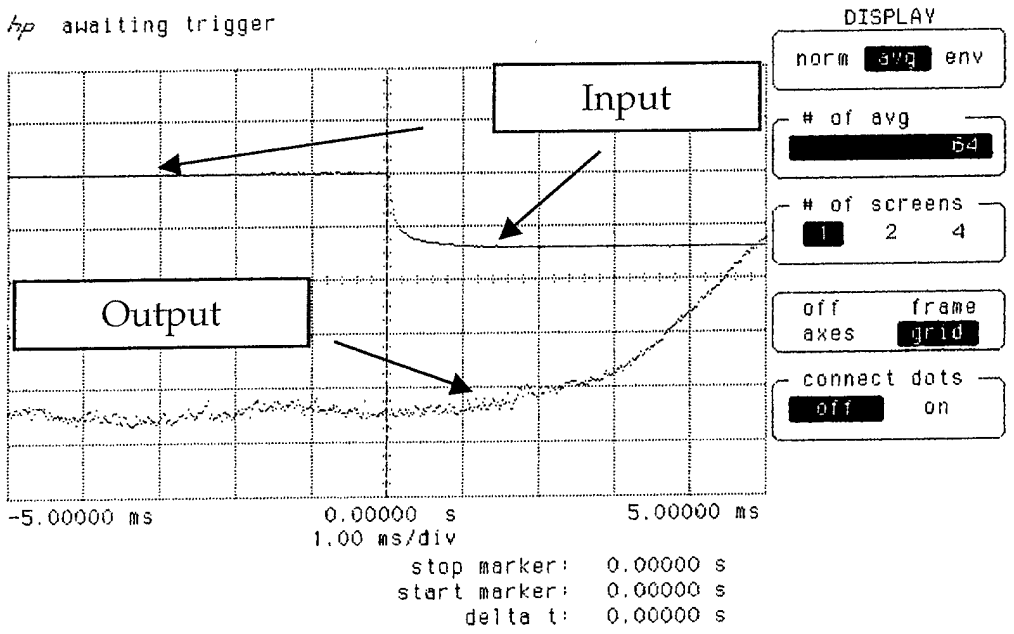

(b)

Figure 18. Response time measured data for T = 30 °C, E = 3kVmm^{-1}, and $\dot{\gamma} = 4 \times 10^3\ s^{-1}$. DC voltage input and tachometer output are shown in (a) and expanded in view of tachometer output in (b) reveals time delay (attributed partly to the ER fluid). Note: traces in (b) correspond to area highlighted by the green rectangle in (a).

6. Recommendations and Conclusions

Results showed that Fluid 1 remained stable over the testing range of electric fields and temperatures. Its activity was near the benchmark criteria. At lower temperatures, the current density was below or near the desired target value. At higher temperatures, above 50 °C, the current density quickly exceeded the target value by factors of five or six. The data also revealed that the fluid has an acceptable zero-field viscosity range above 30 °C. However, because of its fairly high zero-field viscosity below this temperature, future improvements will be necessary, either by reducing the volume fraction of the particles (at the expense of activity), or by using a lighter, less viscous base fluid.

Because of the premature breakdown at relatively low electric fields, it was difficult to realistically assess Fluid 2. Based on the partial data at low electric fields and/or extrapolated results beyond the breakdown conditions, the following conclusions may be drawn. At low temperatures, the current density was about 60% above the desired value. At higher temperatures and high fields, the absolute value of the current density missed the target value by a factor of two. However, the rate of increase of the current density of this fluid (which is presumed to be independent of the fluid breakdown), with respect to temperature, was significantly lower than that of Fluid 1. Fluid 2 met the benchmark criteria in another category, the zero-field viscosity. Finally, extrapolating the high-field activities from those at low fields indicated that high-field activities of a "corrected" fluid (i.e., one that does not break down at intermediate voltages) would also meet the benchmark criteria.

Overall response time measurement results indicated that Fluid 2 was slightly faster than Fluid 1. Within the limited range of test variables, both fluids had activation/deactivation response times of the order of 2.5–3.0 ms for Fluid 1, and about 2.0 ms for Fluid 2. No consistent trend of the response time data was observed for either fluid, with respect to a temperature, shear rate, or field strength variation.

Four fundamental yet undemonstrated aspects of these fluids remain, and they all have a direct impact on implementing the ATLAS program.

(1) The premature settling and sedimentation caused by the remaining density differences between the particulates and the base fluid,

(2) particle abrasion on hydraulic seal integrity,

(3) excessive current drawn resulting in internal overheating and subsequent dielectric breakdown, and

(4) extendibility of the minimum service temperature to well below 0 °C.

Both fluids must be further tested to answer these unresolved issues. Future measurements of the fluid properties must also consider the changing/unchanging properties with repeated cycling and over an extended time period. Additionally, the fluids' compatibility with certain metals, alloys, and polymer-based materials (e.g., copper, titanium alloys, stainless steel, brass, or carbon-epoxy composites) have yet to be addressed.

7. Postscript

Since the writing of this report, the development of improved fluids has continued, and newer formulations/updates from both manufacturers have become available. Based on the manufacturer's specification sheets, fluid properties are beginning to reach the desired goals set forth in Table 1.

The manufacturer of Fluid 2 has released two updates of the same fluid formulation. The first update, released in 1997, was primarily in response to solving and eliminating the cause of the premature breakdown. The cause of the breakdown was related to impurities on the particles and in the base fluid when a switch of material suppliers occurred. The properties of this update were identical to Fluid 2 in most respects, though the activity level was slightly lower than anticipated; the yield strength was about 3 kPa, or 75% of the desired value. A new release became available in 1998, and research has continued through 1999. The new fluid has an acceptable activity level (i.e., near 4 kPa), but with a somewhat higher no-field viscosity at lower temperatures.

The other fluid manufacturer has also produced a new experimental fluid that supposedly has the same characteristics as Fluid 1, but with an activity level that is double the original formulation. All three fluid samples await property verification at ARL.

8. References

1. Kovnat, A. R. "Field Dependent Fluids." Technical Report 13702, U.S. Army Tank-automotive Research, Development, and Engineering Center, Warren, MI, November 1996.
2. Harder, C. R., and D. Wong. "Recoil Arrest With Electrorheological Fluids." ARFSD-CR-94003, U.S. Army Armament Research, Development, and Engineering Center, Picatinny Arsenal, NJ, pp. 21–30, May 1994.
3. Harder, C. R. "Recoil Arrest Control with ER Fluids: Final Report/Addendum." GA-C21324 Addendum, pp. A1–A22, General Atomic Corporation, San Diego, CA, January 1995.
4. Gast, A. P., and C. F. Zukoski. "Electrorheological Fluids as Colloidal Suspensions." *Adv. Colloid and Interfac. Sci.*, vol. 30, pp. 153–202, 1989.
5. Jordan, T. C., and M. T. Shaw. "Electrorheology." *IEEE Trans. Electr. Ins.*, vol. 24, no. 5, pp. 849–878, October 1989.
6. Zukoski, C. F. "Material Properties and the Electrorheological Response." *Ann. Rev. Mater. Sci.*, vol. 23, no. 3–4, pp. 45–78, 1993.
7. Weiss, K. D., J. D. Carlson, and J. P. Coulter. "Material Aspects of Electrorheological Systems." *J. Intell. Mater. Syst. Struct.*, vol. 4, no. 1, pp. 13–34, January 1993.
8. Deneiga, Y. F., and G. V. Vinogradov. "Electric Fields in the Rheology of Disperse Systems." *Rheol. Acta*, vol. 23, no. 6, pp. 636–651, June 1984.
9. Shulman, Z. P., E. V. Korobko, and Y. G. Yanovsky. "The Mechanism of the Viscoelastic Behaviour of Electrorheological Suspension." *J. Non-Newt. Fluid Mech.*, vol. 33, pp. 181–196, 1989.
10. Block, H., and J. P. Kelly. "Electro-Rheology." *J. Phys. D: Appl. Phys.*, vol. 21, no. 12, pp. 1661–1677, December 1988.
11. Winslow, W. M. "Induced Fibrillation of Suspensions." *J. Appl. Phys.*, vol. 20, no. 12, pp. 1137–1140, December 1949.
12. Klass, D. L., and T. W. Martinek. "Electroviscous Fluids I. Rheological Properties." *J. Appl. Phys.*, vol. 38, no. 1, pp. 67–74, January 1967.
13. Klass, D. L., and T. W. Martinek. "Electroviscous Fluids II. Electrical Properties." *J. Appl. Phys.*, vol. 38, no. 1, pp. 75–80, January 1967.
14. Stangroom, J. E. "Electrorheological Fluids." *Phys. Technol.*, vol. 14, pp. 290–296, 1983.

15. Filisko, F. E., and D. R. Gamota. "Electrorheological Materials: Mechanisms and Mechanical Properties." *Recent Advances in Non-Newtonian Flows*, ASME, AMD-vol. 153/PED-vol. 141, pp. 75–86, 1992.

16. Stangroom, J. E. *Electro-Rheological Fluids: An Introduction.* ER Fluid Developments Ltd., Brough, United Kingdom, 1992.

17. Stangroom, J. E. "Basic Observations on Electro-Rheological Fluids." *J. Int. Mater. Syst. Struct.*, vol. 7, no. 9, pp. 479–483, September 1996.

18. Stangroom, J. E. *A Comparison of the Temperature Behaviour of Two ER Fluids.* ER Fluids Developments Ltd., Brough, United Kingdom, 1996.

19. Stangroom, J. E. "The Measurement of the Speed of Response of ER Fluids." *Proceedings of the First International Conference on Electrorheological Fluids*, pp. 81–98, Boston, MA, 1989.

20. Bullough, W. A., J. Makin, A. R. Johnson, A. Hosseini-Sianaki, and R. Firoozian. "ER Shear Characteristics: Volume Fraction, Shear Rate, Time Response." *J. Dyn. Syst. Meas. Contr.*, vol. 118, pp. 221–225, June 1996.

21. Bullough, W. A., A. R. Johnson, J. Makin, R. Tozer, and A. Day. "Status Report: ER Clutch Based Linear Drive." Unpublished data, February 1997.

22. Evans, L. Personal communication. February 1997.

Appendix A. Theory, Governing Relations, and Calibration Method for the Constant-Stress Rheometer

The force balance for the dropweight in the dynamic rig under the combined action of gravity, drag of the bearings, and the viscous force exerted by any fluid between the cup and bob is given as:

$$Ma = Mg - IR^{-2}a - k'v - (\text{viscous torque})R^{-1}.$$

Newtonian Fluid. For a Newtonian liquid in the cup, the viscous force is defined as

$$F_{viscous} = 4\pi h\mu v[R^2(r_1^2 - r_2^2)]^{-1} = D\mu v,$$

where μ is the viscosity, R is the capstan radius, r_1 is the radius of the bob, r_2 is the radius of the cup, h is the bob height, and k'v is the drag term for the bearing. Upon insertion, the relation becomes

$$Ma = Mg - IR^{-2}a - k'v - D\mu v,$$

or

$$a = Mg[M + IR^{-2}]^{-1} - (k' + D\mu)[M + IR^{-2}]^{-1} v.$$

The relationship of a vs. v is linear, with an intercept of

$$a_0 = Mg[M + IR^{-2}]^{-1}$$

and a slope of

$$k = -(k' + D\mu)[M + IR^{-2}]^{-1}.$$

The parameters, called a and k, are calculated by the ERFD's "Lindafit" data reduction program. Lindafit obtains these values directly from the displacement vs. time trajectory.

Bingham Fluid. For a Bingham plastic, the shear stress is defined as

$$\tau = \tau_y + \mu_p \dot{\gamma},$$

where τ_y is yield stress, μ_p is plastic viscosity, and $\dot{\gamma}$ is the shear strain rate. In the absence of an electric field, τ_y is zero, and μ_p is equal to the Newtonian viscosity μ. The derivation for the dynamic viscometer assumes that the fluid is partially shearing. That is, only the portion of fluid is shearing where the yield stress has been exceeded in the gap. When this is inserted into the basic equation, the presence of a yield stress decreases the measured value of a by an amount equal to Δa. The viscosity term remains unchanged and acts through the viscous torque term.

It can be easily shown that for the Bingham fluid

$$\Delta a = 4\pi h r_1^2[2R(M + IR^{-2})]^{-1}\tau_y.$$

Textbooks show that on non-Newtonian fluids (i.e., for conventional and Bingham plastics), when the angular velocity is

$$\Omega = \tau_y \mu_p^{-1}[r_2^2(2r_1)^2 - 0.5 - \ln(r_2 r_1^{-1})],$$

all of the material is being sheared. The term in brackets is 0.0004 for ERFD's system. At τ_y = 3 kPa, μ_p = 150 mPa•s, which leads to a pulse length of 8,000 μs. The first two time-interval pulses usually exceed this on the dynamic rig, but after that the pulses are considerably less (i.e., all of the material is shearing after the first 1–3 pulses).

Calibration Procedure. The calibration procedure is performed using a series of drop-weights and different viscosity oils with Newtonian behavior. Returning to the previous equations for Newtonian fluids, note that the intercept, a_0, is a function only of the weight used, not of the temperature and not of the cup contents. This has been verified by ERFD. Graphs of a_0^{-1} vs. M^{-1} are also linear, and the inertial term can easily be obtained. An absolute calibration may be obtained by verifying that the inverse of the intercept of this plot does correspond to the value of the gravitational constant, g.

The slopes of the calibration lines are

$$k = -k'[M + IR^{-2}]^{-1} - D\mu[M + IR^{-2}]^{-1}.$$

The k values depend on the weight used, as well as on the temperature and type of oil in the cup. (The dependence is through the fluid viscosity, which is a function of temperature.) The remaining unknown terms in this equation can be determined using a series of oils of known viscosity. Based on the previous equation, a graph of k (as calculated by Lindafit) against μ leads to a series of straight lines with an intercept of

$$k'[M + IR^{-2}]^{-1}$$

and slope of

$$D[M + IR^{-2}]^{-1},$$

where

$$D = 4\pi h[R^2(r_1^2 - r_2^2)]^{-1}.$$

Values for the relation of k vs. μ may be refined using these relationships, but are basically drawn directly from the calibration. In the previous equations,

h = bob height = 50 mm,

r_1 = bob radius = 25 mm,

r_2 = cup radius = 25.5 mm,

R = capstan radius = 17.5 mm, and

$M + IR^{-2}$ is already determined during calibration with respect to the dropweight.

The best relation for a 10-lb dropweight from the last calibration of the instrument (performed January 1995) is

$$\mu = (k - 0.419)(0.00375)^{-1},$$

and these constants are temperature independent. The estimated error of μ is about ±10 mPa•s for oils of known viscosity.

As printed from the Lindafit calculation, Δa is angular acceleration, and must therefore be multiplied by the capstan radius (0.0175 m) to give units of ms^{-2}. Working out the relationship for a Bingham fluid,

$$\tau_y\ [kPa] = 10.53 \times 10^{-3}\ \Delta a.$$

It is also clear that when a is 0 (or Δa equals the zero field value of a), the weight will not fall. By calculation, this implies a yield stress of 3.8 kPa. In practice, because of the difference between static and dynamic yield stress, runs with a 10-lb weight cannot measure more than 3.2–3.3 kPa.

Using 18-lb weights will allow measurements of up to 7 kPa. The expected value of a equals 434 ± 10; the calculated yield stress factor equals 16.2×10^{-3}.

INTENTIONALLY LEFT BLANK.

Appendix B. Raw Data From the ERFD Experiments

Table B-1. Fluid 1 current draw.

Run	Temperature (°C)	Field ($kVmm^{-1}$)	Reading (mA)					
			1	2	3	4	5	6
8876	5	0.0	0	0	0	0	0	0
8877	5	0.5	0	0	0	0	0	0
8878	5	1.0	0	0	0	0	0	0
8879	5	1.5	5	5	5	5	5	6
8880	5	2.0	18	16	17	16	17	19
8881	5	2.5	37	34	35	36	38	38
8882	5	3.0	66	62	64	71	76	71
	5	3.0	65					
	5	3.5	94					
	5	4.0	127					
8870	15	0.0	0	0	0	0	0	0
8871	15	0.5	0	0	0	0	0	0
8872	15	1.0	1	2	2	2	2	3
8873	15	1.5	14	13	14	15	15	18
8874	15	2.0	37	39	41	40	45	42
8875	15	2.5	76	85	82	87	93	87
	15	3.0	147					
	15	3.5	208					
	15	4.0	278					
8802	30	0.0	0	0	0	0	0	0
8803	30	0.5	0	0	0	0	0	0
8804	30	1.0	22	29	27	29	28	27
8805	30	1.5	103	103	110	108	107	103
8806	30	2.0	211	259	238	223		
8807	30	2.0	256	256	254	266	230	225
8808	30	2.5	435	402	385	414	402	415
8809	30	3.0	663	623	648	599	660	612
8810	30	3.5	854	884	818	889	833	892
	30	4.0	1140					
8811	40	0.0	0	0	0	0	0	0
8812	40	0.5	0	0	0	0	0	0
8813	40	1.0	42	51	55	56	54	51
8814	40	1.5	198	180	186	195	178	186
8815	40	2.0	404	459	388	406	437	378

Table B-1. Fluid 1 current draw (continued).

Run	Temperature (°C)	Field ($kVmm^{-1}$)	Reading (mA)					
			1	2	3	4	5	6
8816	40	2.5	658	684	619	648	699	688
8817	40	3.0	931	1038	1105	987	1015	1110
8818	40	3.5	1370	1280	1390	1280	1420	1290
8819	40	4.0	1800					
8819	50	0.0	0	0	0	0	0	0
8820	50	0.5	15	19	21	20	19	25
8821	50	1.0	229	203	224	209	224	220
8822	50	1.5	592	682	681	699	676	644
8823	50	2.0	1170	1350	1300	1210	1260	1420
8824	50	2.5	1910	2330	2290	2240	2120	2090
8825	50	3.0	3600	3460	3300	3440	3280	3430
	50	3.5	5000					
8826	60	0.0	0	0	0	0	0	0
8827	60	0.5	58	68	75	75	80	61
8828	60	1.0	475	571	581	615	608	585
8829	60	1.5	1580	1470	1600	1620	1620	1680
8830	60	2.0	3570	2960	3520	3050		

Table B-2. Fluid 1 yield stress.

Run	Temperature (°C)	Field ($kVmm^{-1}$)	k	a	Max Velocity (rad/s)
8876	5	0.0	1.173	347.8	111.4
8877	5	0.5	1.523	328.2	110.4
8878	5	1.0	1.597	321.8	107.7
8879	5	1.5	1.461	292.4	103.3
8880	5	2.0	1.487	281.3	100.7
8881	5	2.5	1.108	243.0	99.0
8882	5	3.0	0.937	215.7	94.8
	5	3.0			
	5	3.5			
	5	4.0			
8870	15	0.0	1.416	340.2	115.8
8871	15	0.5	1.274	331.4	116.2
8872	15	1.0	1.370	323.5	113.0
8873	15	1.5	1.121	291.4	110.0
8874	15	2.0	0.987	276.0	110.0
8875	15	2.5	1.002	260.3	105.7
	15	3.0			
	15	3.5			
	15	4.0			
8802	30	0.0	0.898	344.5	127.2
8803	30	0.5	0.876	337.9	125.8
8804	30	1.0	0.750	310.6	123.3
8805	30	1.5	0.597	286.5	120.2
8806	30	2.0			
8807	30	2.0	0.181	223.9	112.1
8808	30	2.5	0.485	208.9	102.7
8809	30	3.0	-0.094	132.4	90.8
8810	30	3.5	-0.037	97.5	76.7
		4.0			
8811	40	0.0	0.396	321.4	131.8
8812	40	0.5	0.544	323.5	129.0
8813	40	1.0	0.549	306.4	125.4
8814	40	1.5	0.391	269.0	120.1
8815	40	2.0	0.604	248.9	111.7
8816	40	2.5	1.010	236.3	100.6
8817	40	3.0	0.304	142.4	86.8
8818	40	3.5	-0.003	83.7	70.7

Table B-2. Fluid 1 yield stress (continued).

Run	Temperature (°C)	Field ($kVmm^{-1}$)	k	a	Max Velocity (rad/s)
8819	40	4.0			
8819	50	0.0	0.712	339.9	129.6
8820	50	0.5	0.413	312.7	129.3
8821	50	1.0	0.543	301.9	125.2
8822	50	1.5	0.491	259.1	115.8
8823	50	2.0	0.572	220.4	104.3
8824	50	2.5	0.559	179.1	93.0
8825	50	3.0	0.416	121.2	77.1
	50	3.5			
	50	4.0			
8826	60	0.0	0.451	345.2	136.0
8827	60	0.5	0.300	320.7	133.2
8828	60	1.0	0.513	303.6	126.1
8829	60	1.5	0.349	254.5	117.2
8830	60	2.0	-0.705	193.9	109.1

Table B-3. Fluid 2 current draw.

Run	Temperature (°C)	Field ($kVmm^{-1}$)	Reading (mA)						
			1	2	3	4	5	6	
8883	5	0.0	0	0	0	0	0	0	
8884	5	0.5	23	24	23	24	25	25	
8885	5	1.0	84	83	87	89	87	88	
8886	5	1.5	177	179	177	174	182	181	
8887	5	2.0	282	283	285	288	298	298	
8888	5	2.5	433	424	435	452	454	446	
	5	3.0	592	590	602	606			
8858	15	0.0	0	0	0	0	0	0	
8859	15	0.5	32	32	33	32	34	32	
8860	15	1.0	110	108	110	112	113	115	
8861	15	1.5	222	225	228	222	232	236	
8862	15	2.0	375	372	378	385	385	389	
	15	2.5	552	565	552	572	583	575	
8831	30	0.0	0	0	0	0	0	0	
8832	30	0.5	55	57	57	58	55	56	
8833	30	1.0	189	187	186	191	192	196	
8834	30	1.5	368	372	396	391	377	387	
8835	30	2.0	616	615	626	615	656		
8836	40	0.0	0	0	0	0	0	0	
8837	40	0.5	71	75	75	76	77	75	
8838	40	1.0	241	250	251	253	246	250	
8839	40	1.5	476	483	486	475	498	480	
8840	40	2.0	790	794	765	779	804	777	
8841	40	2.5	1121	1119					
8843	40	3.0	1460	1510	1440	1460			
8842	40	2.5	1070	1080	1100	1080	1090	1100	
8844	40	3.0	1460	1500	1460	1480			
8845	40	0.0	0	0	0	0	0	0	Degassed
8846	40	0.5	74	75	76	75	75	75	Degassed
8847	40	1.0	249	254	256	251	247	245	Degassed
8848	40	1.5	488	490	495	495	508		Degassed
8849	40	2.0	785	777	805	810	818	815	Degassed
8850	40	2.5	1100	1120	1110	1130			Degassed
	40	3.0	1530						Degassed
	40	3.5	1990						Degassed
	40	4.0	2540						Degassed
8851	50	0.0	0	0	0	0	0	0	

Table B-3. Fluid 2 current draw (continued).

Run	Temperature (°C)	Field ($kVmm^{-1}$)	Reading (mA)						
			1	2	3	4	5	6	
8852	50	0.5	99	105	104	101	104	102	
8853	50	1.0	322	328	321	324	324		
8855	50	1.5	633						
8854	50	1.0	323	314	316	329	332	317	
	50	2.0	1008						
	50	2.5	1400						
	50	3.0	1880						
	50	3.5	2420						
	50	4.0	3030						
8856	60	0.0	0	0	0	0	0	0	
8857	60	0.5	136	141	134	142	138	140	
	60	1.0	440	448	444	440	451	442	
	60	1.5	833						
	60	2.0	1290						
	60	2.5	1830						
	60	3.0	2460						
	60	3.5	3140						
	60	4.0	3900						

Table B-4. Fluid 2 yield stress.

Run	Temperature (°C)	Field ($kVmm^{-1}$)	k	a	Max Velocity (rad/s)	
8883	5	0.0	0.640	343.0	131.2	
8884	5	0.5	0.655	340.6	130.8	
8885	5	1.0	0.431	317.5	130.1	
8886	5	1.5	0.220	289.5	128.5	
8887	5	2.0	0.163	267.4	124.6	
8888	5	2.5	-0.218	207.2	117.8	
	5	3.0				
8858	15	0.0	0.710	341.6	129.6	
8859	15	0.5	0.886	356.2	129.5	
8860	15	1.0	0.530	322.4	129.2	
8861	15	1.5	0.093	275.8	127.0	
8862	15	2.0	-0.122	235.0	125.8	
	15	2.5				
8831	30	0.0	0.738	359.6	133.4	
8832	30	0.5	0.588	342.2	131.3	
8833	30	1.0	0.561	329.6	131.9	
8834	30	1.5	0.350	297.9	128.7	
8835	30	2.0	-0.050	236.7	120.7	
8836	40	0.0	0.562	356.1	136.1	
8837	40	0.5	0.431	340.2	134.4	
8838	40	1.0	0.346	323.0	133.2	
8839	40	1.5	-0.087	264.5	129.0	
8840	40	2.0	-0.123	231.0	122.0	
8841	40	2.5	-0.551	173.4	114.8	
8843	40	3.0	0.026	161.7	99.8	
8842	40	2.5	-0.049	196.7	111.9	
8844	40	3.0	-0.505	138.2	98.7	
8845	40	0.0	0.533	332.5	131.4	Degassed
8846	40	0.5	0.505	330.6	131.4	Degassed
8847	40	1.0	0.350	309.6	130.7	Degassed
8848	40	1.5	-0.376	234.4	125.5	Degassed
8849	40	2.0	0.016	229.6	119.0	Degassed
8850	40	2.5	-0.581	156.2	109.4	Degassed
	40	3.0				Degassed
	40	3.5				Degassed
	40	4.0				Degassed
8851	50	0.0	0.499	351.7	136.8	
8852	50	0.5	0.353	338.4	135.9	

Table B-4. Fluid 2 yield stress (continued).

Run	Temperature (°C)	Field ($kVmm^{-1}$)	k	a	Max Velocity (rad/s)	
8853	50	1.0	0.527	338.3	132.0	
8855	50	1.5				
8854	50	1.0	0.360	331.3	137.9	
	50	2.0				
	50	2.5				
	50	3.0				
	50	3.5				
	50	4.0				
8856	60	0.0	0.286	345.1	139.4	
8857	60	0.5	0.455	357.1	138.6	
	60	1.0				
	60	1.5				
	60	2.0				
	60	2.5				
	60	3.0				
	60	3.5				
	60	4.0				

NO. OF COPIES	ORGANIZATION
2	DEFENSE TECHNICAL INFORMATION CENTER DTIC OCA 8725 JOHN J KINGMAN RD STE 0944 FT BELVOIR VA 22060-6218
1	HQDA DAMO FDT 400 ARMY PENTAGON WASHINGTON DC 20310-0460
1	OSD OUSD(A&T)/ODDR&E(R) DR R J TREW 3800 DEFENSE PENTAGON WASHINGTON DC 20301-3800
1	COMMANDING GENERAL US ARMY MATERIEL CMD AMCRDA TF 5001 EISENHOWER AVE ALEXANDRIA VA 22333-0001
1	INST FOR ADVNCD TCHNLGY THE UNIV OF TEXAS AT AUSTIN 3925 W BRAKER LN STE 400 AUSTIN TX 78759-5316
1	DARPA SPECIAL PROJECTS OFFICE J CARLINI 3701 N FAIRFAX DR ARLINGTON VA 22203-1714
1	US MILITARY ACADEMY MATH SCI CTR EXCELLENCE MADN MATH MAJ HUBER THAYER HALL WEST POINT NY 10996-1786
1	DIRECTOR US ARMY RESEARCH LAB AMSRL D DR D SMITH 2800 POWDER MILL RD ADELPHI MD 20783-1197

NO. OF COPIES	ORGANIZATION
1	DIRECTOR US ARMY RESEARCH LAB AMSRL CI AI R 2800 POWDER MILL RD ADELPHI MD 20783-1197
3	DIRECTOR US ARMY RESEARCH LAB AMSRL CI LL 2800 POWDER MILL RD ADELPHI MD 20783-1197
3	DIRECTOR US ARMY RESEARCH LAB AMSRL CI IS T 2800 POWDER MILL RD ADELPHI MD 20783-1197
	ABERDEEN PROVING GROUND
2	DIR USARL AMSRL CI LP (BLDG 305)

NO. OF COPIES	ORGANIZATION
1	HQDA SARD TR WASHINGTON DC 20301
1	CDR US ARMY RSCH OFC PO BOX 12211 RSCH TRIANGLE PARK NC 27709-2211
5	CDR US ARMY ARDEC SMCAR TDC M CHIEFA S CYTRON R ESPINOSA S FLOROFF PICATINNY ARSENAL NJ 07806-5000
1	DIR BENET LABS SMCAR CCB TL WATERVLIET NY 12189
1	CDR US ARMY AMCCOM SMCAR ESP L ROCK ISLAND IL 61299
1	CDR US ARMY FOREIGN SCIENCE & TECHNICAL CTR 220 SEVENTH ST NE CHARLOTTESVILLE VA 22901
4	DIR BRIDGESTONE FIRESTONE RESEARCH G BOHM PRODUCT PROCESSING RSCH J RENSEL W NIAURA P PAKDEL S MAIN & WILBERTH AKRON OH 44317-0001
2	GENERAL ATOMICS CORP ELECTROMAGNETIC SYS C HARDER M TABOR 3550 GENERAL ATOMICS CT SAN DIEGO CA 92121-1122

NO. OF COPIES	ORGANIZATION
	ABERDEEN PROVING GROUND
33	DIR USARL AMSRL R WHALIN J ROCCHIO E SCHMIDT AMSRL WM M D VIECHNICKI G HAGNAUER J BEATTY B FINK W ROY R SHUFORD AMSRL WM P J BOYD W DOUSA H ROGERS J WALL L BURTON AMSRL WM T B BURNS A NIILER A CARDAMONE AMSRL WM MD K ANDERSON L KECSKES (15 CPS)

NO. OF COPIES	ORGANIZATION
3	DIR ER FLUID DEVELOPMENTS LTD L EVANS P KERMODE I HARNESS VINCENT WORKS BROUGH BRADWELL HOPE VALLEY SHEFFIELD S30 2HG UNITED KINGDOM

INTENTIONALLY LEFT BLANK.

REPORT DOCUMENTATION PAGE

Form Approved
OMB No. 0704-0188

1. AGENCY USE ONLY *(Leave blank)*	2. REPORT DATE	3. REPORT TYPE AND DATES COVERED
	May 2001	Final, February 1997–June 1998

4. TITLE AND SUBTITLE
Assessment of Two Electro-Rheological Fluids for Use in Recoil Abatement Applications

5. FUNDING NUMBERS
IL622105AH84-622105A

6. AUTHOR(S)
Laszlo J. Kecskes

7. PERFORMING ORGANIZATION NAME(S) AND ADDRESS(ES)
U.S. Army Research Laboratory
ATTN: AMSRL-WM-MD
Aberdeen Proving Ground, MD 21005-5069

8. PERFORMING ORGANIZATION REPORT NUMBER
ARL-TR-2483

9. SPONSORING/MONITORING AGENCY NAMES(S) AND ADDRESS(ES)

10.SPONSORING/MONITORING AGENCY REPORT NUMBER

11. SUPPLEMENTARY NOTES

12a. DISTRIBUTION/AVAILABILITY STATEMENT
Approved for public release; distribution is unlimited.

12b. DISTRIBUTION CODE

13. ABSTRACT*(Maximum 200 words)*

The electrical and rheological properties of two state-of-the-art electro-rheological (ER) fluids have been evaluated from 0 to 60 °C, using a unique constant-stress viscometer. The measurements were performed at the facilities of ER Fluid Developments, Ltd. (ERFD), a small British company located in Sheffield, United Kingdom, that specializes in developing and marketing ER fluid-based technology. In addition to these measurements, the response time of the fluids was determined using another instrument located at the nearby University of Sheffield.

The constant-stress viscometer, or dynamic rig, developed and owned by ERFD, permits the yield stress, plastic viscosity, and direct current (DC) current density of an ER fluid to be determined as a function of electric field and temperature. The yield stress, plastic viscosity, current density, and response time of each fluid were found to strongly depend on temperature. The first fluid appears to be stronger (i.e., has a higher yield stress), with lower current densities at lower temperatures up to 40 °C. In that temperature range, the second fluid is somewhat weaker, susceptible to electrical breakdown at or above 2.0 $kVmm^{-1}$, and generally draws more current. At higher temperatures, however, the current density of the first fluid dramatically increases to exceed the desired level of 10 μAcm^{-2}. The corresponding current density increase of the second fluid is significantly smaller. In light of the differences between the measured properties, the results and their implications associated with the intended use of the fluids are discussed. A general description of ER fluid behavior, as well as the theories of operation of the instruments, are also described.

14. SUBJECT TERMS
ER effect, shear stress, yield stress, plastic viscosity, current density, reponse time

15. NUMBER OF PAGES
58

16. PRICE CODE

17. SECURITY CLASSIFICATION OF REPORT	18. SECURITY CLASSIFICATION OF THIS PAGE	19. SECURITY CLASSIFICATION OF ABSTRACT	20. LIMITATION OF ABSTRACT
UNCLASSIFIED	UNCLASSIFIED	UNCLASSIFIED	UL

INTENTIONALLY LEFT BLANK.

USER EVALUATION SHEET/CHANGE OF ADDRESS

This Laboratory undertakes a continuing effort to improve the quality of the reports it publishes. Your comments/answers to the items/questions below will aid us in our efforts.

1. ARL Report Number/Author ARL-TR-2483 (Kecskes) Date of Report May 2001

2. Date Report Received _____

3. Does this report satisfy a need? (Comment on purpose, related project, or other area of interest for which the report will be used.) _____

4. Specifically, how is the report being used? (Information source, design data, procedure, source of ideas, etc.) _____

5. Has the information in this report led to any quantitative savings as far as man-hours or dollars saved, operating costs avoided, or efficiencies achieved, etc? If so, please elaborate. _____

6. General Comments. What do you think should be changed to improve future reports? (Indicate changes to organization, technical content, format, etc.) _____

CURRENT ADDRESS

_____
Organization

_____
Name E-mail Name

_____
Street or P.O. Box No.

_____
City, State, Zip Code

7. If indicating a Change of Address or Address Correction, please provide the Current or Correct address above and the Old or Incorrect address below.

OLD ADDRESS

_____
Organization

_____
Name

_____
Street or P.O. Box No.

_____
City, State, Zip Code

(Remove this sheet, fold as indicated, tape closed, and mail.)

(DO NOT STAPLE)

DEPARTMENT OF THE ARMY

OFFICIAL BUSINESS

NO POSTAGE
NECESSARY
IF MAILED
IN THE
UNITED STATES

BUSINESS REPLY MAIL
FIRST CLASS PERMIT NO 0001,APG,MD

POSTAGE WILL BE PAID BY ADDRESSEE

DIRECTOR
US ARMY RESEARCH LABORATORY
ATTN AMSRL WM MD
ABERDEEN PROVING GROUND MD 21005-5066